Stem Cell Reports
Article

ISSCR

OPEN ACCESS

The Dlg Module and Clathrin-Mediated Endocytosis Regulate EGFR Signaling and Cyst Cell-Germline Coordination in the *Drosophila* Testis

Fani Papagiannouli,[1,2,*] Cameron Wynn Berry,[1] and Margaret T. Fuller[1]
[1]Department of Developmental Biology, Beckman Center, Stanford University School of Medicine, Stanford, CA 94305-5329, USA
[2]Institute for Genetics, University of Cologne, 50674 Cologne, Germany
*Correspondence: fani.papagiannouli@alumni.uni-heidelberg.de
https://doi.org/10.1016/j.stemcr.2019.03.008

SUMMARY

Tissue homeostasis and repair relies on proper communication of stem cells and their differentiating daughters with the local tissue microenvironment. In the *Drosophila* male germline adult stem cell lineage, germ cells proliferate and progressively differentiate enclosed in supportive somatic cyst cells, forming a small organoid, the functional unit of differentiation. Here we show that cell polarity and vesicle trafficking influence signal transduction in cyst cells, with profound effects on the germ cells they enclose. Our data suggest that the cortical components Dlg, Scrib, Lgl and the clathrin-mediated endocytic (CME) machinery downregulate epidermal growth factor receptor (EGFR) signaling. Knockdown of *dlg*, *scrib*, *lgl*, or CME components in cyst cells resulted in germ cell death, similar to increased signal transduction via the EGFR, while lowering EGFR or downstream signaling components rescued the defects. This work provides insights into how cell polarity and endocytosis cooperate to regulate signal transduction and sculpt developing tissues.

INTRODUCTION

The genesis and maintenance of functional tissues and organs require close communication between disparate cell types, with exchange of short-range signals regulating cell proliferation and survival, cell fate, and local patterning. Tissues or highly differentiated cell types with a high turnover rate such as intestinal epithelium, red blood cells, or skin rely on adult stem cells for constant replenishment of differentiated cell populations (Monahan and Starz-Gaiano, 2016). Tissue homeostasis and repair by adult stem cell lineages rely on equilibrium of stem cell maintenance versus differentiation guided by short-range communication with the local microenvironment (Losick et al., 2011; Matunis et al., 2012; Papagiannouli and Lohmann, 2012).

In *Drosophila*, male germline stem cells (GSCs) reside at the apical tip of the testis, flanked by somatic cyst stem cells (CySCs), maintained through their association with the hub, a cluster of normally non-dividing somatic cells forming the niche organizer (Figure 1A). By asymmetric cell division, each GSC produces a new GSC attached to the hub plus a distally located gonialblast (GB). The GB initiates four rounds of transit-amplifying (TA) mitotic divisions with incomplete cytokinesis, giving rise to 2, 4, 8, and eventually 16 interconnected spermatogonial germ cells. Immediately after reaching the 16-cell stage, germ cells undergo a final round of DNA synthesis, enter meiotic prophase, and turn on the spermatocyte transcription program for meiosis and spermatid differentiation. The somatic CySCs also divide asymmetrically, producing CySCs that remain associated with the hub plus distally located post-mitotic daughters that become cyst cells (Fuller and Spradling, 2007). Two somatic cyst cells enclose each GB, forming a two-cell squamous epithelium that encases the mitotic and meiotic progeny of that GB throughout the rest of male germ cell differentiation until sperm individualization. Notably, the cyst cells co-differentiate with the germ cells they enclose (Gonczy and DiNardo, 1996), support germ cell differentiation (Lim and Fuller, 2012), and control spermatogenesis from initial differentiation to mature sperm production (Leatherman, 2013; Zoller and Schulz, 2012).

Signals from the germline to the cyst cells via the epidermal growth factor (EGF) play a major role in spermatogenesis (Hudson et al., 2013; Kiger et al., 2000; Sarkar et al., 2007; Schulz et al., 2002; Tran et al., 2000). Activation of the EGF receptor (EGFR) and its downstream signal transduction pathway, leading to phosphorylation of mitogen-activated protein kinase (MAPK) in the cyst cells, is required for germ cells to properly enter and execute the mitotic proliferation program of synchronous TA divisions that is the first step of differentiation (Kiger et al., 2000; Sarkar et al., 2007; Schulz et al., 2002; Tran et al., 2000). Activation of the EGFR on cyst cells at even higher levels is required for germ cells to exit the mitotic proliferation program and switch to the spermatocyte state (Hudson et al., 2013).

Here we show that function of the cell polarity components *discs large* (*dlg*), *scribble* (*scrib*), and *lethal* (*2*) *giant larvae* (*lgl*) in the cyst cell lineage are crucial for proper formation of a functional cyst microenvironment that supports the survival of differentiating germ cells. *dlg*, *scrib*, and *lgl* were first identified as tumor-suppressor genes, loss of function of which led to neoplastic transformation (Bilder and Perrimon, 2000; Donohoe et al., 2018; Goode

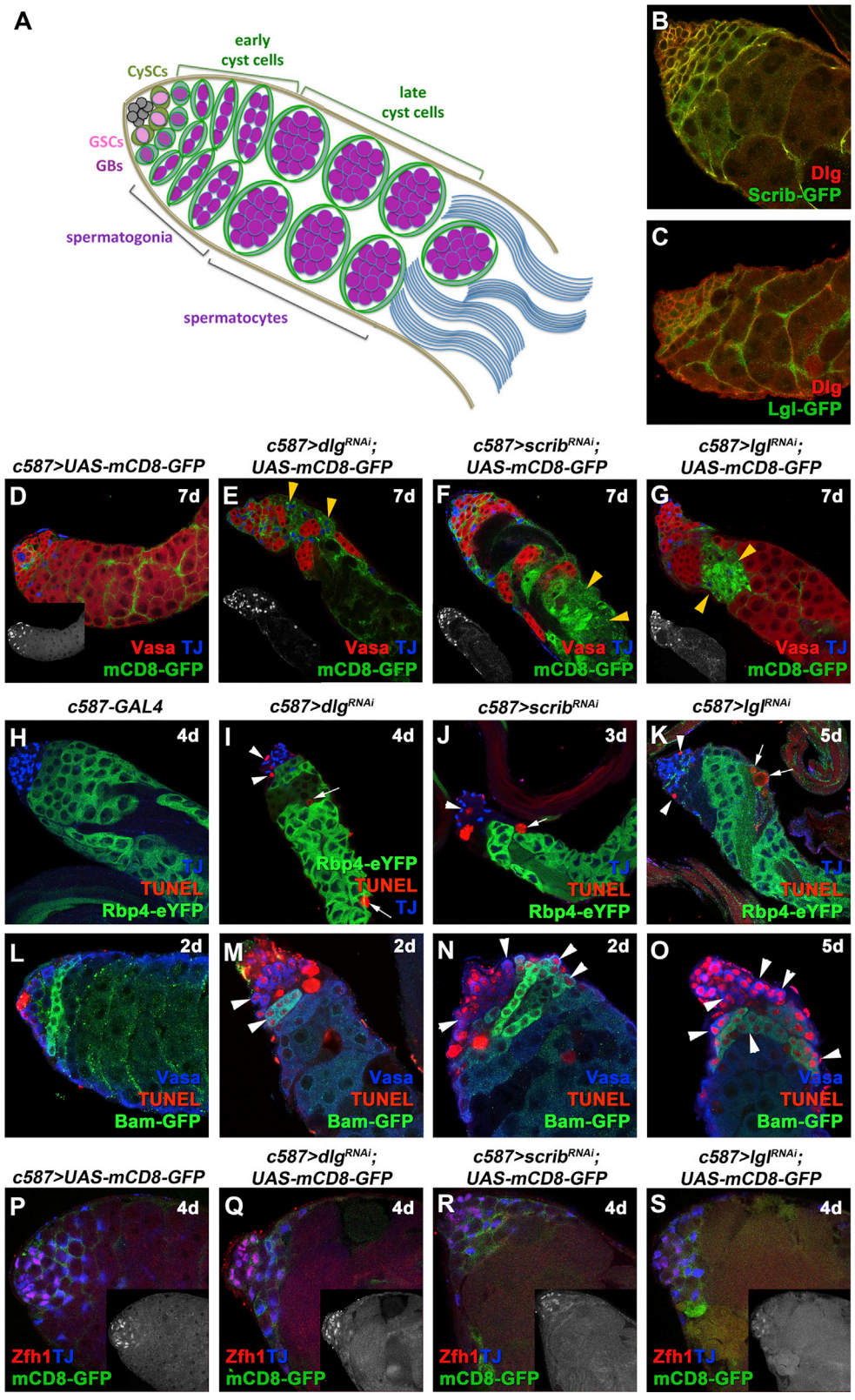

(legend on next page)

and Perrimon, 1997; Humbert, 2015; Li et al., 2001; Woods et al., 1996). Dlg, Scrib, and Lgl, collectively called the Dlg module, are highly conserved polarity and scaffolding proteins involved in: (1) establishment and maintenance of apical/basal cell polarity in columnar epithelia in cooperation with the Par- (Bazooka/Par3, Par6, αPKC) and Crumbs-polarity complexes; (2) vesicle and membrane trafficking in *Drosophila*, yeast, and mammals; and (3) cooperation with signaling pathways (e.g., Ras, Notch, JNK) in normal tissues and in cancer (de Vreede et al., 2014; Gui et al., 2016; Humbert, 2015; Parsons et al., 2014; Roegiers et al., 2005; Uhlirova and Bohmann, 2006). Previous work showed that somatic cells fail to extend projections and encapsulate the germ cells in embryonic gonads of male flies mutant for *scrib* or *dlg*, suggesting a role in establishing intimate germline-soma contacts (Marhold et al., 2003; Papagiannouli, 2013). Larval and adult males mutant for *dlg*, *scrib*, or *lgl* have extremely small testes with reduced number of GSCs, accumulation of cyst cells, and impaired germ cell differentiation, resulting in sterility (Fairchild et al., 2017; Papagiannouli, 2013; Papagiannouli and Mechler, 2009). Importantly, expression of a *dlg* transgene in cyst cells of *dlg* mutant larval testes rescued encapsulation of the germline by somatic cells and the architecture and integrity of spermatogonial and spermatocyte cysts (Papagiannouli and Mechler, 2009).

Our results suggest that the highly conserved Dlg module cooperates with clathrin-mediated endocytic (CME) components to downregulate the EGFR signaling in somatic cyst cells. We show that cell-type-specific knockdown of the Dlg module or CME components in cyst cells results in increased levels of downstream mediators of EGFR signaling, accompanied by non-autonomous germ cell death, phenocopying the effect of EGFR overactivation in cyst cells. Lowering the levels of EGFR signal transduction components in cyst cells partially rescued the observed defects and restored germ cell survival in animals with loss of Dlg-module or CME-component function in cyst cells, while the membrane phospholipid phosphatidylinositol 4,5-bisphosphate (PIP_2) contributed to MAPK activation. Our results suggest that the Dlg module and endocytosis normally downregulate signaling via the EGFR and that this fine-tuning is critical for proper and stepwise differentiation of germline cysts.

RESULTS

Knockdown of *dlg*, *scrib*, or *lgl* Function in Cyst Cells Leads to Germ Cell Death

Dlg, Scrib, and Lgl are co-expressed in early cyst cells that encapsulate GBs and spermatogonia, and late cyst cells that enclose spermatocyte cysts (Figures 1B and 1C). Function of Dlg-module components was impaired in the cyst cell lineage using the *c587-GAL4* driver with *UAS-gene^{RNAi}* lines to knock down expression of *dlg*, *scrib*, or *lgl*. Flies also carried an *αtubGal80^{ts}* transgene, which blocks *GAL4* activity at 18°C but not at 30°C, allowing acute downregulation of gene function in adults, after normal testis anatomy had been set up. Analysis of the tissue 2, 4, or 7 days after the shift to 30°C allowed us to observe progression of the phenotypes over time (e.g., Figure S1).

Knockdown of *dlg*, *scrib*, or *lgl* function in cyst cells had non-autonomous effects on differentiating germ cells, resulting in loss of spermatogonia and spermatocytes. Germ cell loss was visible as a gap in Vasa staining (Figures 1E–1G) that became progressively larger with longer exposure to knockdown conditions (Figures S1A–S1D″), while in control testes Vasa marked all densely packed germ cells (Figure 1D). TUNEL staining revealed dying spermatocytes (marked by expression of an Rbp4-YFP transgene) and spermatogonia (Figures 1H–1K) undergoing apoptosis in testes with cyst cells depleted of *dlg*, *scrib*, or *lgl* function. Since cell-type-specific markers were no longer visible in late apoptotic stages, TUNEL staining was also performed at 2 days of knockdown to score cell death activation in early (Vasa$^+$) spermatogonia and late spermatogonia, marked by expression of a late spermatogonial Bam-GFP transgene (Bam$^+$/Vasa$^+$) (Figures 1L–1O). At 2-day knockdown TUNEL staining marked the initial activation of apoptosis in the majority of spermatogonia (Figures 1M–1O; white arrowheads), while at 3–4 days of knockdown TUNEL

Figure 1. Knockdown of *dlg*, *scrib*, or *lgl* Function in Cyst Cells Leads to Cell Non-autonomous Germ Cell Death

(A) Diagram of early spermatogenesis in *Drosophila*. GSC, germline stem cell; GB, gonialblast; CySC, somatic cyst stem cell.

(B and C) Adult testes from flies endogenously tagged with (B) Scrib-GFP or (C) Lgl-GFP immunostained stained for Dlg (red) and GFP (green). Adult testes of the indicated genotypes in the *Gal80^{ts}* background.

(D–G) *mCD8-GFP* (green; cyst cells), Vasa (red; germline), and TJ (blue; early cyst cell nuclei). Small inset pictures show the TJ staining. Yellow arrowheads indicate mCD8$^+$ cyst cell regions.

(H–O) TJ (blue), TUNEL (red; apoptosis), and GFP (green; Rbp4-YFP$^+$ spermatocytes or Bam$^+$ spermatogonia). White arrowheads indicate dying spermatogonia, White arrows indicate dying spermatocytes.

(P–S) *mCD8-GFP* (green; cyst cells), Zfh1 (red; CySC and immediate daughters), and TJ (blue). Small inset pictures show the Zfh1 staining. RNAi activated at 30°C for 2, 3, 4, 5, or 7 days (d). Testes oriented with anterior at left. Image frames, 246 μm (D–K) and 123 μm (B, C, and L–S). See also Figures S1 and S2.

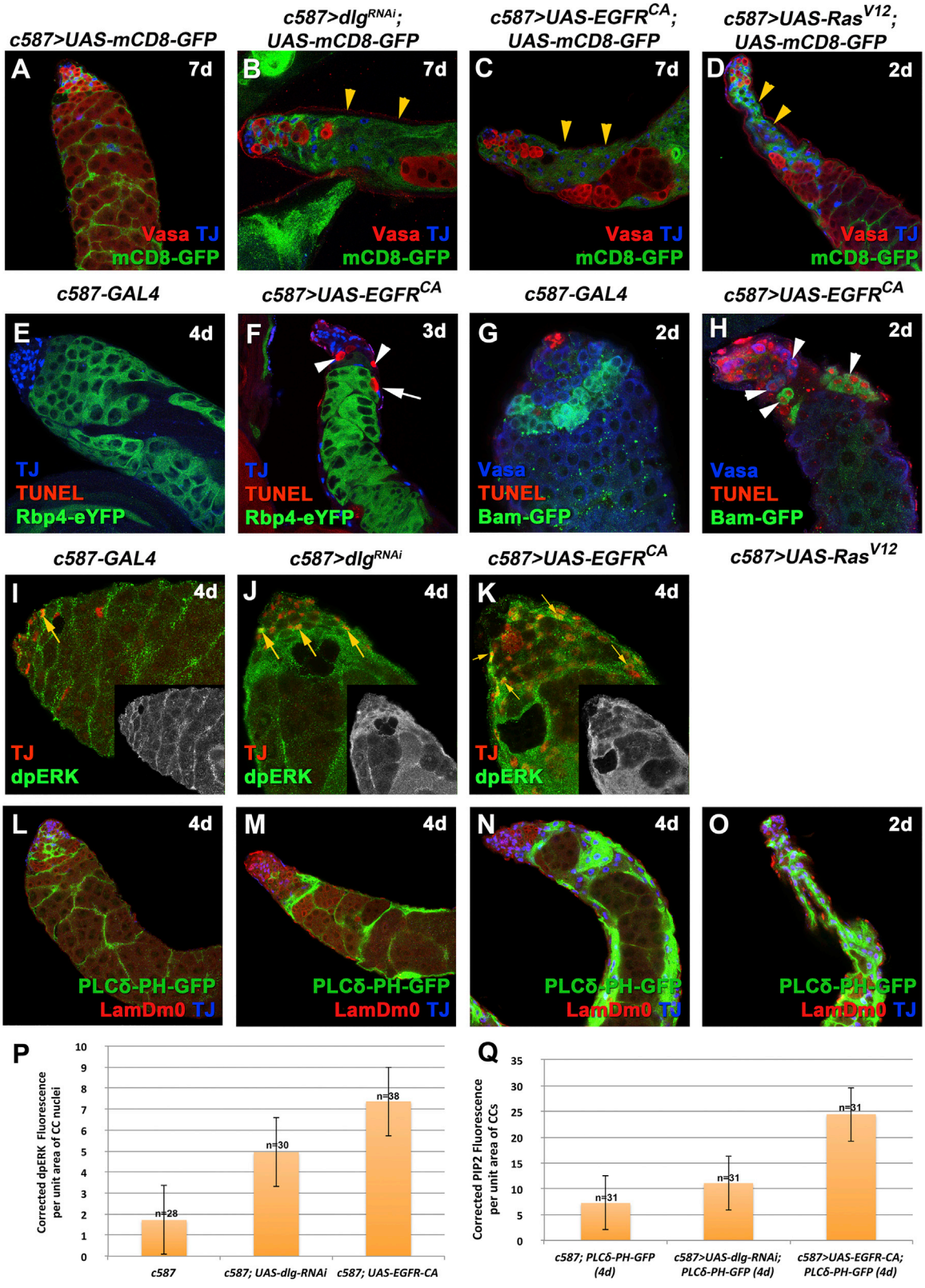

(legend on next page)

marked the remaining spermatogonial (Figures 1H–1K; arrowheads) and spermatocyte (Figures 1H–1K; arrows) cysts, visible as red blebs devoid of cell-type-specific markers at a more advanced stage of apoptosis.

Even after 7 days of knockdown, testes typically contained early spermatogonia that, based on staining for phosphorylated histone 3 (PH3), retained their capacity to proliferate (Figures S2A–S2D) and produced at least some cysts of germ cells positive for the late spermatogonial marker Bam (Figures S2E and S2G–S2I′). After 5 days of *dlg*, *scrib*, or *lgl* knockdown in cyst cells only few Rbp4$^+$ spermatocyte cysts remained (Figures S1N–S1P).

The loss of germ cells was accompanied by clustering of the *dlg*, *scrib*, or *lgl* depleted cyst cells in the affected regions, visible as patches of the membrane CD8-GFP (mCD8-GFP) marker expressed in cyst cells (Figures 1D–1G). At 2-day knockdown, the defects appeared initially around TJ-positive early cyst cells that clustered together as germ cells first began to be eliminated (Figures S1A–S1D). The mCD8$^+$ patches progressively expanded (Figures S1A′–S1D″; yellow arrowheads) as germ cell loss continued at 4 and 7 days' knockdown. Double knockdown of *dlg* with *scrib* or *lgl* led to phenotypes similar to the single knockdowns (Figures S1E–S1H), in agreement with the Dlg-module proteins acting along the same pathway.

Knockdown of *dlg*, *scrib*, or *lgl* function in the cyst cell lineage did not appear to alter cyst cell identity. Immunostaining for Zfh1, which marks CySCs and their immediate daughter cyst cells (Leatherman and Dinardo, 2008), showed Zfh1$^+$ nuclei clustered at the apical tip of testes, as in the wild type (Figures 1P–1S). Likewise, cyst cells positive for the early cyst cell marker TJ but Zfh1-negative were ranked farther from the hub than the Zfh1$^+$ cyst cells in knockdown testes, as in the wild type (Figures 1P–1S).

Loss of *dlg*, *scrib*, or *lgl* Causes Defects Similar to Overactivation of the EGFR Pathway

The phenotype resulting from suppression of *dlg*, *scrib*, or *lgl* function in cysts cells strongly resembled the phenotype cause by constitutively active EGFR (EGFR^{CA}) (Hudson et al., 2013 and Figure 2C) or *Ras85D* (*UAS-Ras^{V12}*) (Singh et al., 2016 and Figure 2D) in cyst cells. Immunostaining of adult testes overexpressing either *UAS-EGFR^{CA}* or *UAS-Ras85D^{V12}* in cyst cells revealed that early germ cells near the testis tip persisted, while some Bam$^+$ late spermatogonial cysts were still formed (Figures S2Q–S2S), which retained their proliferation capacity (Figure S2F). Slightly farther from the testis tip, cyst cells (lacking associated germ cells) accumulated as clusters of TJ$^+$ nuclei embedded in mCD8-GFP patches (Figures 2C and 2D). TUNEL staining of testes 2–3 days after forced expression of *UAS-EGFR^{CA}* showed dying germ cells within the Rbp4$^+$ spermatocyte region (Figure 2F), and in Vasa$^+$/Bam$^-$ and Bam$^+$ spermatogonia (Figure 2H), similar to that observed after knockdown of Dlg-module components in cyst cells (Figures 1H–1O). By 5 days of knockdown, only a few Rbp4$^+$ spermatocytes remained (FiguresS2Q and S2S). Importantly, overexpression of a wild-type form of EGFR or *Ras85D* in cyst cells resulted in milder phenotypes (Figures S2R, S3B, and S3C) reminiscent of the defects observed after only 2 days of knockdown of *dlg*, *scrib*, or *lgl* (compare Figures S1B–S1D with S3B and S3C).

Strikingly, knockdown of *dlg*, *scrib*, or *lgl* in cyst cells resulted in elevated levels of phosphorylated MAPK (dpERK), a canonical downstream effector of the EGFR signal transduction pathway. In testes co-stained for dpERK and the early cyst cell marker TJ, cyst cells depleted for *dlg*, *scrib*, or *lgl* or overexpressing *EGFR^{CA}* showed increased dpERK levels in TJ$^+$ cyst cell nuclei compared with nuclei of similarly staged cyst cells in control testes (Figures 2I–2K, 2P, S3D–S3F, and S3J).

As EGFR activation can also result in elevated levels of the membrane phospholipid PIP_2 (Czech, 2000), we assessed PIP_2 levels in cyst cells by expressing the PLCδ-PH-GFP reporter, which contains the PIP_2-specific pleckstrin-homology domain of phospholipase Cδ (Gervais et al., 2008). Levels of the PIP_2 reporter appeared higher in testes in which cyst cells were depleted for *dlg*, *scrib*, and *lgl* function

Figure 2. Knockdown of *dlg*, *scrib*, or *lgl* and Overactivation of EGFR Signaling in Cyst Cells Have Similar Phenotypes

Adult testes of the indicated genotypes in the *Gal80^{ts}* background.

(A–D) *mCD8-GFP* (green; cyst cells), Vasa (red; germline), and TJ (blue; early cyst cell nuclei). Yellow arrowheads indicate mCD8$^+$ cyst cell regions.

(E–H) TJ (blue), TUNEL (red; apoptosis), and GFP (green; Rbp4-YFP$^+$ spermatocytes or Bam-GFP$^+$ spermatogonia). White arrowheads indicate dying spermatogonia. White arrows indicate dying spermatocytes.

(I–K) TJ (red) and dpERK (green). Yellow arrows indicate examples of cyst cells double-labeled for TJ and dpERK. Small inset pictures show the dpERK staining.

(L–O) The PIP_2 reporter PLCδ-PH-GFP expressed in cyst cells (green), LamDm0 (red; cyst cells and early germ cells), and TJ (blue).

(P) Quantification of corrected fluorescent dpERK levels in cyst cell (CC) nuclei.

(Q) Quantification of corrected fluorescent PIP_2 levels in cyst cells (CC) via the PLCδ-PH-GFP reporter.

Error bars represent standard error. RNAi activated at 30°C for 2, 3, 4, or 7 days (d). Testes oriented with anterior at left. Image frames, 246 μm (A–F and L–O) and 123 μm (G–K). See also Figures S2 and S3.

or were overexpressing $EGFR^{CA}$ and Ras^{V12}, compared with control testes (Figures 2L–2O, 2Q, S3G–S3I, and S3K).

Lowering Levels of EGFR Signal Transduction Pathway Components in Cyst Cells Partially Rescues *dlg*, *scrib*, and *lgl* Knockdown Phenotypes

Given the enhanced dpERK activity following *dlg*, *scrib*, or *lgl* inhibition, we tested whether reduced EGFR signaling might rescue the Dlg-module knockdown phenotypes. Strong loss of EGFR function results in failure of cyst cells to encapsulate early spermatogonia and defects in the ability of germ cells to properly enter the TA program of four rounds of synchronous mitotic divisions (Kiger et al., 2000; Sarkar et al., 2007; Schulz et al., 2002; Tran et al., 2000). As a result, early spermatogonia of mixed identity proliferate extensively and the cyst cells are pushed to the testis periphery. To circumvent the extreme early phenotype caused by a complete EGFR loss, we took three different approaches to interfere with the EGFR signaling. We lowered the gene dose by using flies heterozygous for the null $EGFR^{K05115}$ allele ($EGFR^{K05115/+}$) (Figures 3C and S4D1–S4D3), and overexpressed a dominant negative EGFR allele (*UAS-*$EGFR^{DN}$) (Figure 4B), or transgenic RNAi to knock down the EGFR (*UAS-*$EGFR^{RNAi}$) or Ras (*UAS-*Ras^{RNAi}) in the background of *dlg*, *scrib*, and *lgl* knockdowns in cyst cells.

To control for possible effects of multiple UAS constructs limiting the effectiveness of the *GAL4* driver or multiple RNAi constructs limiting the effectiveness of the RNAi machinery, we set up control flies to carry the same number of *UAS* transgenes using two types of controls: *UAS-mCD8-GFP* or *UAS-eGFP-RNAi*. Because different *UAS* transgenes have different expression strengths, rescue experiments were performed by shifting flies to 30°C for 4, 5, and 7 days.

The observed phenotypes were classified into the following categories: (1) "dlg LOF" included testes that mimicked the effect of acute *dlg* cyst cell knockdown, with strong decrease in number of germ cells (comparable with Figures 1E, 2B, S1B′, and S1B″) but also very weak knockdowns where only small patches of cyst cell clusters devoid of germ cells were identified (comparable with Figures S1B–S1D); (2) "wt" for testes with restored spermatogonial and spermatocyte cysts similar to wild type; and (3) "EGFR LOF" for all phenotypes that resulted in overproliferation of early spermatogonia resembling loss of EGFR signaling. Representative examples of the different phenotypic classes, reflecting the variability in strength and penetrance of "dlg LOF" and "EGFR LOF" phenotypic classes in comparison with "wt" for the different genotypes, are shown in Figures 3 and S4.

Although a range of phenotypes resulted from our rescue strategy, the percentage of testes showing a "dlg LOF" phenotype was substantially reduced, usually to less than 50%, by lowering EGFR function in cyst cells in which Dlg-module components had been knocked down (Figures 3 and S4). In many cases 50% or more of the testes scored showed packed spermatogonial and spermatocyte cysts, and restored architecture as in the wild type. With 7 days of exposure to knockdown conditions, the strong "EGFR LOF" phenotype of overproliferating spermatogonial cysts came to predominate in some genotypes (Figure 3M). Lowering the function of MAPK, encoded by the *Drosophila rolled* (*rl*) gene, also partially rescued *dlg*-module loss-of-function phenotypes in cyst cells (Figures S5A–S5M).

Effects of Loss of CME in Cyst Cells Resemble Loss of Dlg-Module Components

The amplitude and specificity of signaling levels is generally regulated by endocytosis of activated receptors that can either recycle back to the cell surface or be transported to lysosomes for degradation (Goh and Sorkin, 2013). EGFR becomes endocytosed mainly by CME (Conte and Sigismund, 2016). Given the significance of CME in EGFR signaling attenuation, we investigated whether loss of CME components in cyst cells affects EGFR signaling levels. Knockdown of the CME components *shibire/shi* (*Drosophila* homolog of *dynamin*), *AP-2α* (also known as *α-Adaptin*), or *Clathrin heavy chain* (*Chc*) in cyst cells recapitulated the *dlg*, *scrib*, or *lgl* cyst cell knockdown and EGFR overactivation phenotypes, suggesting that EGFR signaling is attenuated by endocytosis in cyst cells (Figure 4). As seen after knockdown of Dlg-module components, testes in which *shi*, *AP-2α*, or *Chc* was depleted in the cyst cell lineage retained $Vasa^+$ germ cells at the testis tip (Figures 4B–4D), produced some proliferating Bam^+ spermatogonia (Figures S2J–S2L and S2T–S2V), and had $Zfh1^+$ and $TJ^+/Zfh1^-$ cyst cell nuclei ranked at the testis apical tip, suggesting that the identity of early cyst cells remained intact and comparable with wild-type controls (Figures S2W–S2Z). However, away from the testis tip, testes depleted for *shi*, *AP-2α*, or *Chc* function showed TJ^+ cyst cell nuclei clustered in mCD8-GFP-positive regions devoid of germ cells (Figures 4A–4D), and germ cell death. TUNEL staining confirmed that both $Vasa^+/Bam^-$ and Bam^+ spermatogonia (Figures 4I–4L) and $Rbp4^+$ spermatocytes underwent cell death (Figures 4E–4H).

Similar to knockdown of Dlg-module components, inhibition of *shi*, *AP-2α*, or *Chc* function resulted in increased levels of dpERK in TJ^+ cyst cell nuclei (Figures 4M–4Q) and elevated levels of PIP_2 as assessed by the PLCδ-PH-GFP reporter (Figures 4R–4V). Double knockdown of *dlg* with *shi*, *AP-2α*, or *Chc* led to phenotypes similar to those of the single knockdowns (Figures S1I–S1M), suggesting that CME and the Dlg module act along the same pathway.

Lowering EGFR signaling levels by expressing *UAS-*$EGFR^{DN}$ in cyst cells (Figures 5B, 5E, and 5H) or by

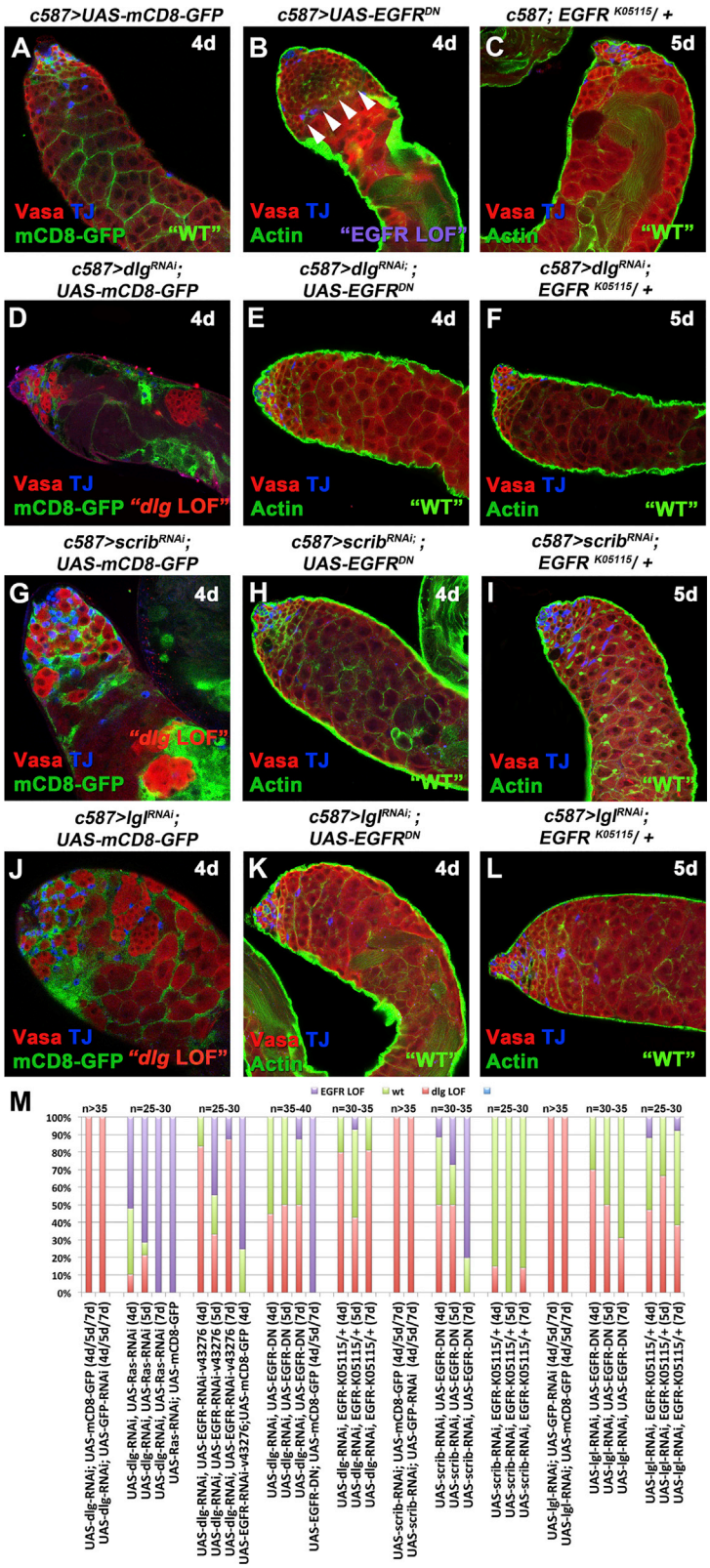

Figure 3. Lowering EGFR Signaling Levels Can Rescue the *dlg*, *scrib*, and *lgl* Knockdown Phenotypes in Cyst Cells

(A–L) Adult testes of the indicated genotypes in the *Gal80^{ts}* background: Vasa (red; germline), TJ (blue; early cyst cell nuclei), and either actin stained with phalloidin (green; cyst cells and germline fusome) or *mCD8-GFP* (green; cyst cells). White arrowheads indicate over-proliferating early spermatogonia.

(M) Quantifications of the different phenotypic classes accompanying each genotype, organized in order of phenotypic strength.

RNAi activated at 30°C for 4 or 5 days (d). Testes oriented with anterior at left. Image frames, 246 μm. See also Figures S4 and S5.

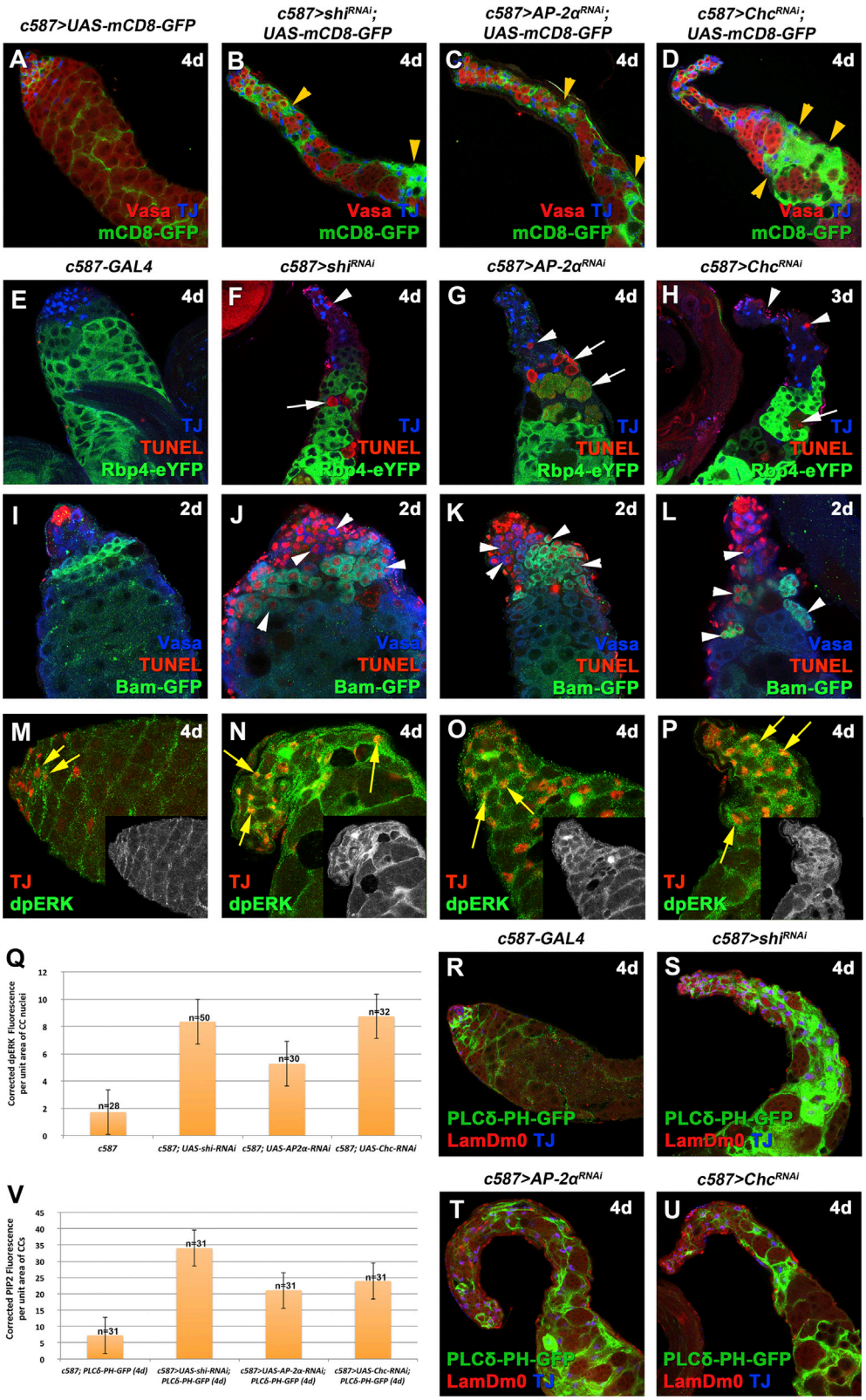

(legend on next page)

removing one copy of the null $EGFR^{K05115}$ allele (Figures 5C, 5F, and 5I) rescued the phenotypes caused by knockdown of *shi*, *AP-2α*, or *Chc* in cyst cells (Figure 5K). Rescue experiments were scored according to four phenotypic classes: (1) "dlg LOF" included testes that mimicked the *dlg* cyst cell knockdown phenotypes, with strong decrease in number of germ cells (comparable with Figures 1E, 2B, S1B′, and S1B″); (2) "partial rescue/dlg weak" included very weak knockdown phenotypes with only small patches of cyst cell clusters devoid of germ cells (comparable with Figures S1B–S1D) and germ cells filling up the majority of the testis; (3) "wt" for testes with restored spermatogonial and spermatocyte cysts as in the wild type; and (4) "EGFR LOF" for all phenotypes that resulted in overproliferation of early spermatogonia resembling loss of EGFR signaling. When $EGFR^{DN}$ was overexpressed along with *shi*, *AP-2α*, or *Chc* cyst cell knockdown, less than 10% of the testes scored showed the CME loss-of-function phenotype, and many testes showed packed spermatogonia and spermatocytes resembling wild type or EGFR loss-of-function overproliferation of spermatogonia (Figures 5K and S6). Removing one copy of the null $EGFR^{K05115}$ allele also rescued testes in *shi*, *AP-2α*, or *Chc* cyst cell knockdowns, although the rescue was much weaker than for $EGFR^{DN}$ overexpression, as expected (Figure 5K).

Knocking down the function of Rab11 in cyst cells, part of the regulatory machinery for the recycling endosome, led to phenotypes resembling strong EGFR loss of function (Figures S5Q and S5R), suggesting that recycling of internalized EGFR back to the plasma membrane is necessary to maintain proper levels of EGFR activity in cyst cells. Consistently, knocking down Rab11 in *dlg*-depleted cyst cells partially rescued the *dlg* loss-of-function phenotype (Figures S5O and S5P), as seen for reducing EGFR signaling levels by other means.

Sktl/dPIP5K Regulates dpERK Levels in Cyst Cells

Cyst cell knockdown of the *Drosophila skittles* (*sktl*) gene, encoding the dPIP5K kinase that synthesizes PIP_2 from phosphatidylinositol 4-kinase (Balakrishnan et al., 2015; Gervais et al., 2008), reduced the severity of Dlg-module or CME-component knockdown and of the $EGFR^{CA}$ overexpression phenotypes (Figures 6B–6H and 6S). The dramatic germline apoptosis normally observed in Dlg-module and CME-component knockdown in cyst cells, was reversed in many of the testes scored (Figure 6S), and staining for filamentous actin (F-actin) revealed that cyst cells could encapsulate again groups of germ cells containing branched fusomes (Figures 6B–6H). Interestingly, staining with phosphorylated MAPK (Figures 6I–6Q) revealed that dpERK levels in TJ^+ cyst cells were significantly reduced to almost wild-type levels (Figure 6R), suggesting that both CME and PIP_2 contribute to MAPK activation.

Dlg-Module and CME Components Share Common and Distinct Characteristics with Septate Junction Components

The Dlg-module proteins regulate polarity across different tissues (Humbert, 2015), while Dlg and Scrib localize at the cytoplasmic side of septate junctions (SJs), and in imaginal discs Dlg promotes the correct localization of the core SJ complex (Oshima and Fehon, 2011). To address the potential connection to SJs and polarity, we analyzed the function of the SJ core component Coracle (Cora) (Fehon et al., 1994) and compared the effects with the Dlg module, CME components, and EGFR in cyst cells. Knockdown of *cora* in cyst cells for 4 days resulted in loss of late spermatogonia (Fairchild et al., 2015; Figures 7B and 7C), accompanied by clustering of *cora*-depleted cyst cells in $mCD8^+$ regions. In longer knockdowns of 5–7 days, $mCD8^+$ patches progressively expanded as germ cell loss continued and *cora*-depleted testes typically retained few early spermatogonia clustering only around the niche (Figures S7B, S7C, S7B′, and S7C′). This was in contrast to the Dlg-module and CME-component knockdowns or EGFR overactivation, in which the remaining germ cells retained their capacity to proliferate (Figures S2A–S2L) and produced at least some cysts away from the niche (compare Vasa

Figure 4. Defects in CME Show Similar Phenotypes as Loss of Function of Dlg Module or EGFR Overactivation in Cyst Cells

Adult testes of the indicated genotypes in the $Gal80^{ts}$ background.

(A–D) *mCD8-GFP* (green; cyst cells), Vasa (red; germline), and TJ (blue; early cyst cell nuclei). Yellow arrowheads indicate $mCD8^+$ cyst cell regions.

(E–L) TJ (blue), TUNEL (red; apoptosis), and GFP (green; $Rbp4\text{-}YFP^+$ spermatocytes or $Bam\text{-}GFP^+$ spermatogonia). White arrowheads indicate dying spermatogonia. White arrows indicate dying spermatocytes.

(M–P) TJ (red) and dpERK (green). Yellow arrows indicate examples of TJ^+ and $dpERK^+$ cyst cells. Small inset pictures show the dpERK staining.

(Q) Quantification of corrected fluorescent dpERK levels in cyst cell (CC) nuclei.

(R–U) The PIP_2 reporter PLCδ-PH-GFP expressed in cyst cells (green), LamDm0 (red; cyst cells and early germ cells), and TJ (blue).

(V) Quantification of corrected fluorescent PIP_2 levels in cyst cells (CC) via the PLCδ-PH-GFP reporter.

Error bars represent standard error. RNAi activated at 30°C for 2, 3, or 4 days (d). Testes oriented with anterior at left. Image frames, 246 μm (A–H and R–U) and 123 μm (I–P). See also Figures S1 and S2.

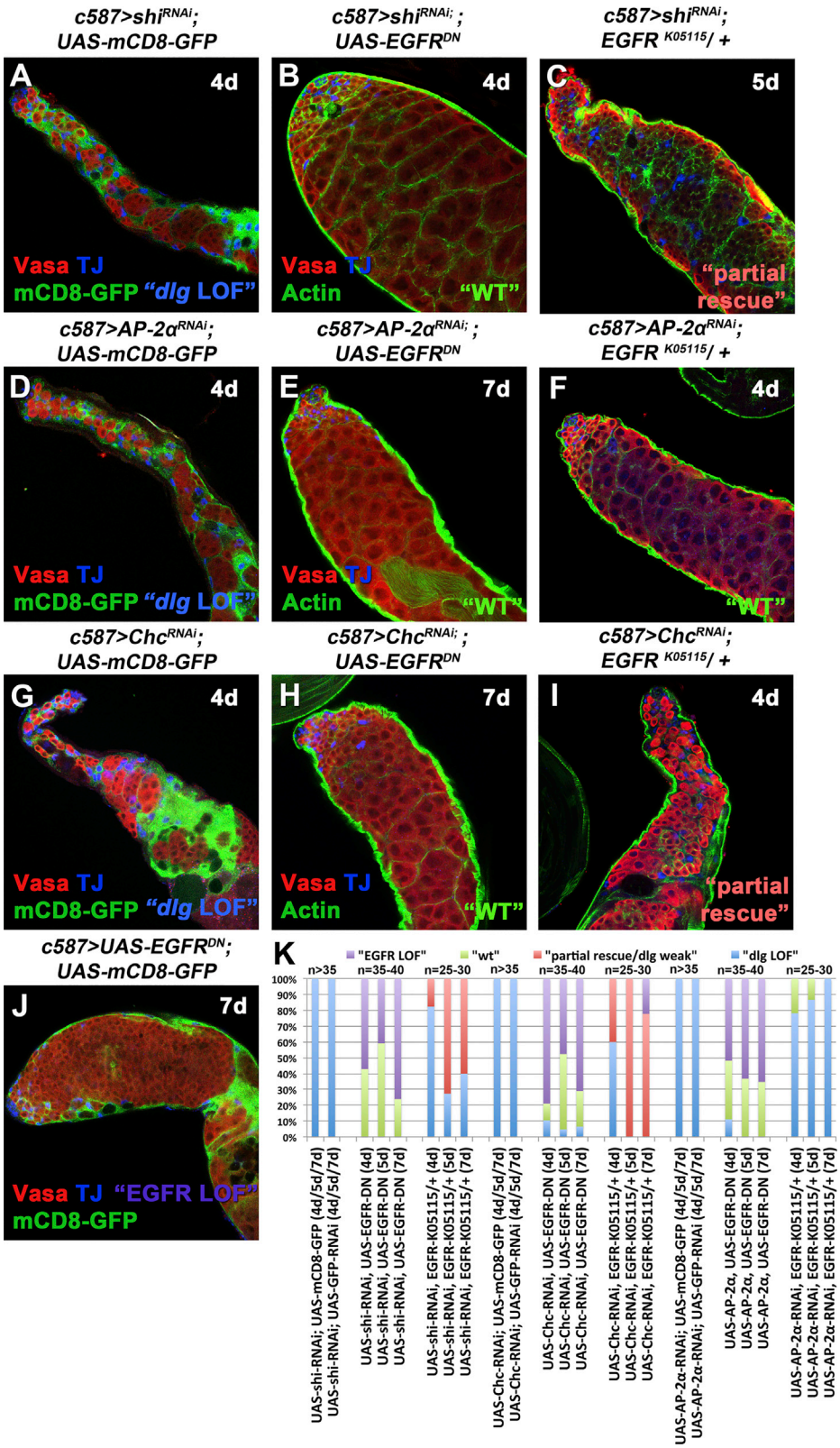

(legend on next page)

staining in Figures S7B′, S7C′ with S1B″, S1C″, S2B–S2D, and 4B–4D). Similar to knockdown of Dlg-module and CME components, inhibition of *cora* function in cyst cells resulted in increased levels of dpERK in TJ^+ cyst cell nuclei (Figures 7E, 7F, and 7J), while downregulation of the EGFR signaling pathway partially rescued the *cora* loss-of-function phenotype as germ cell death was reversed and testis contained densely packed spermatogonia and spermatocyte cysts (Figures 7D, 7I, and S7D–S7D′). Moreover, *cora*-depleted cyst cells showed elevated levels of the PIP_2 reporter PLCδ-PH-GFP (Figures 7G, 7H, and 7K), but this was restricted in early cyst cells surrounding spermatogonia, unlike the Dlg-module and CME-component knockdowns or EGFR overactivation in which increased PIP_2 levels were also observed in late cyst cells surrounding dying spermatocytes (compare Figure 7H with Figures 2M–2O, S3H, S3I, and 4S–4U).

To assay whether loss of *dlg*, *scrib*, or *lgl* in *Drosophila* testis cyst cells was associated with changes in polarity, we investigated the localization of the adherens junction component α-Catenin (α-Cat) and the basal SJ protein NeurexinIV (NrxIV). Knockdown of Dlg-module and CME components or EGFR overactivation in cyst cells showed no loss or obvious changes in α-Cat (Figures S7E–S7L) or NrxIV (Figures 7L–7O and S7M–S7Q). However, as the elongated squamous cyst cells clustered together (devoid of the dying germ cells they normally encapsulate), we could not conclude whether α-Cat or NrxIV were mislocalized in apical versus basal cyst cell membranes.

To bypass this problem, we assayed for potential changes in epithelial integrity of the cyst cells following an alternative strategy. SJs in the *Drosophila* testis are critical for establishing occluding junctions that form an isolating permeability barrier around the germ cells they encapsulate, and loss of basal polarity is often associated with increased permeability and defective functionality of the barrier (Fairchild et al., 2015). The permeability barrier is normally established at 4-cell stage spermatogonial cysts at the contact sides of the two cyst cells constituting the cyst and becomes fully functional at spermatocyte stage, as dextran dyes can no longer access the spermatocytes (Fairchild et al., 2015). Using a dextran dye we tested whether the permeability of the testis barrier was affected in Dlg-module, *cora*, and CME-component knockdowns or upon EGFR overactivation in cyst cells (Figures 7P–7Y and S7R–S7X). The results showed that EGFR overactivation or loss of *cora* function in cyst cells resulted in complete loss of the permeability barrier as the dextran dye could fully penetrate the majority of spermatocyte cysts (Figure 7Q and 7X). Although downregulation of EGFR signaling pathway in *cora*-depleted cyst cells could largely rescue germ cell death and restore the spermatogonial and spermatocyte cysts (Figures 7D and S7D–S7D′), it could not restore the function of the barrier with the dextran dye entering the majority of spermatocyte cysts (Figure 7Y). On the other hand, knockdown of the Dlg-module or CME components in cyst cells led to milder permeability defects, with dextran dye entering fewer spermatocyte cysts by forming localized small indentations between the spermatocytes (Figures 7R, 7T, 7V, S7R, S7U, and S7W). Moreover, lowering EGFR signaling in cyst cells depleted of Dlg-module or CME-component function largely restored the integrity of the permeability barrier (Figures 7S, 7U, 7W, S7S, S7T, S7V, and S7X) with only occasional permeability defects, seen as small dextran indentations between neighboring spermatocytes (Figures 7U, S7S, and S7T, yellow arrowheads).

DISCUSSION

Male gamete development requires close communication between germline and neighboring somatic cells. Our results indicate that the cortical cell polarity and scaffolding proteins Dlg, Scrib, and Lgl, and components of CME play an important role in the intimate germline-cyst cell signaling exchange that sets up a functional microenvironment required for proper differentiation of early germ cells. Our findings show that loss of *dlg*, *scrib*, *lgl*, or CME components in the cyst cells results in phenotypes resembling overactivation of the EGFR signaling pathway, including non-cell-autonomous effects on germ cells leading to death of spermatogonia and spermatocytes. Lowering activity of EGFR signaling components in cyst cells partially rescued and restored these defects, indicating that the Dlg module and CME can fine-tune the EGFR pathway activity in cyst cells, either through effects on signal transduction downstream of EGFR activation or internalization of the receptor (Figure 7Y).

Sequential steps in early male germ cell differentiation in *Drosophila* require increasing levels of EGFR activation in cyst cells (Hudson et al., 2013). Receipt of EGF signaling from the germline promotes encapsulation of the GB by two cyst cells (Sarkar et al., 2007; Schulz et al., 2002), and

Figure 5. Lowering EGFR Signaling Levels Can Rescue CME Defects in Cyst Cells

(A–J) Adult testes of the indicated genotypes in the *Gal80^{ts}* background: Vasa (red; germline), TJ (blue; early cyst cell nuclei), and either *mCD8-GFP* (green; cyst cells) or F-actin stained with phalloidin (green; cyst cells and germline fusome).

(K) Quantifications of the different phenotypic classes accompanying each genotype, organized in order of phenotypic strength.

RNAi activated at 30°C for 4, 5, or 7 days (d). Testes oriented with anterior at left. Image frames, 246 μm. See also Figures S5 and S6.

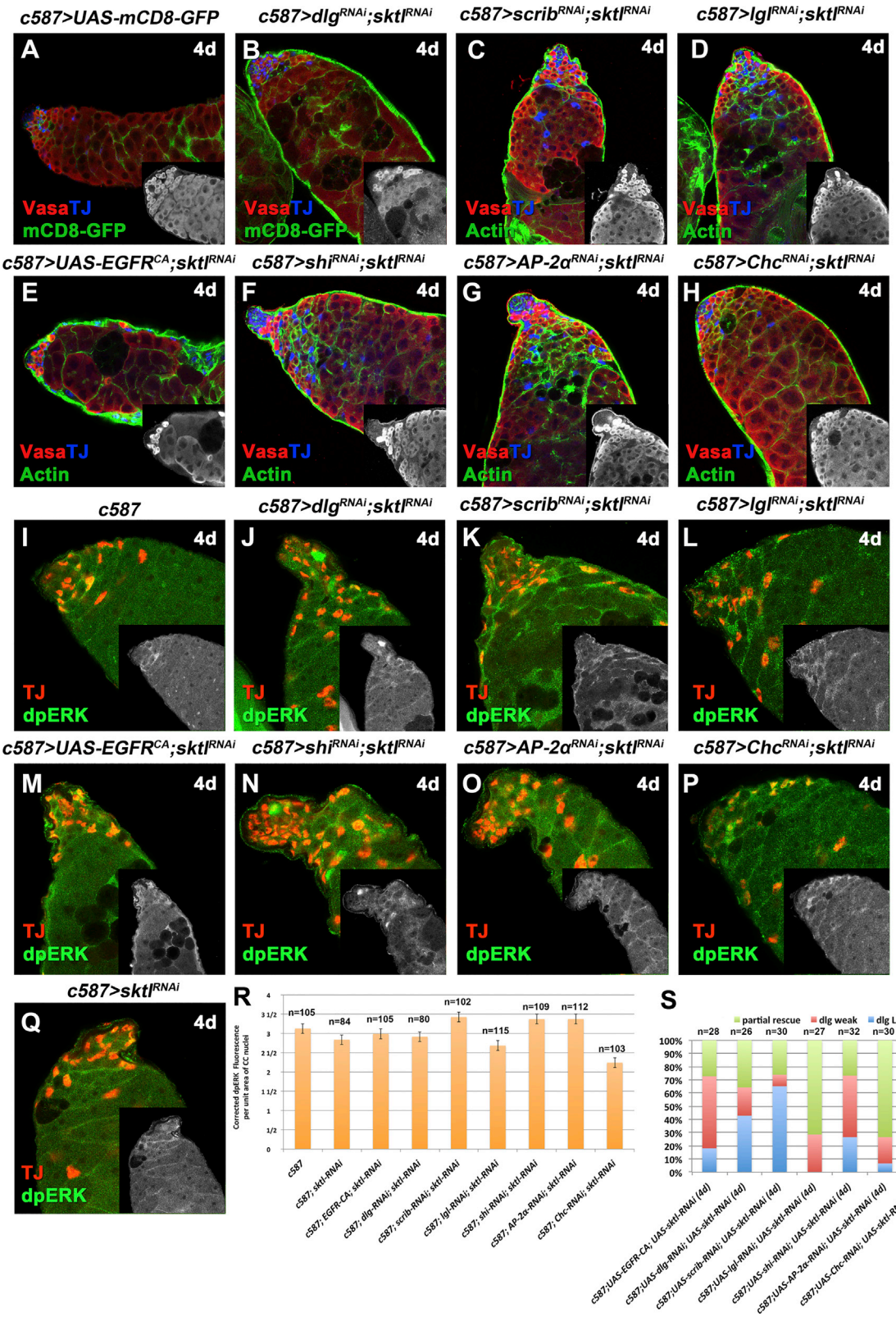

(legend on next page)

consequent activation of the EGFR on cyst cells is required for germ cells to properly enter the TA program of synchronous mitotic divisions (Kiger et al., 2000; Tran et al., 2000). Higher levels of EGFR activation in cyst cells are required for spermatogonia to end the TA divisions and initiate the spermatocyte program (Hudson et al., 2013). Our data show that EGFR signaling in cyst cells affects the survival of the germline and the integrity of the permeability barrier. The death of spermatogonia and spermatocytes we observe may depend on cyst cells experiencing very highly sustained levels of EGFR activation sending mixed or stage inappropriate signals to the germ cells they enclose. The germ cell death seems to be more differentially regulated than the maintenance of the permeability barrier, as illustrated in *cora*-depleted cyst cells, in which lowering EGFR signaling levels restores the viability of the germline but not the integrity of the permeability barrier.

Attenuation of EGFR signaling via endocytosis has been demonstrated in many tissues and organs across species, and deregulation of this process is implicated in cancer initiation and progression (Conte and Sigismund, 2016; Goh and Sorkin, 2013). Upon binding of EGF ligand, the EGFR becomes activated by phosphorylation and recruits adaptor proteins that stimulate the Ras/MAPK cascade. However, EGFR phosphorylation also stimulates internalization of the EGFR receptor, mainly by CME (Conte and Sigismund, 2016; Czech, 2000; Goh and Sorkin, 2013). Activated EGFR is recruited to clathrin-coated pits by interacting with the adaptor protein 2 (AP-2) complex, after which clathrin-coated pits invaginate and pinch off with the action of the GTPase Dynamin, encoded by the *shibire* gene in *Drosophila* (Chen et al., 2002; Conte and Sigismund, 2016; Goh and Sorkin, 2013). Knockdown of any of these CME components in the cyst cell lineage resulted in phenotypes resembling those caused by forced overactivation of the EGFR or Ras in cyst cells, suggesting that CME is required to maintain levels of EGFR signaling in a range appropriate for the normal developmental progression of male germline cysts. The internalized EGFR is generally targeted for degradation or recycled back to the plasma membrane. The fact that Rab11 in cyst cells can rescue the *dlg* loss-of-function defects raises the possibility that recycling the EGFR back to the membrane is critical to keep EGFR signaling active and in a physiological range.

The Dlg module could act to attenuate signaling via the EGFR in cyst cells either by potentiating endocytosis of the receptor or, independently of CME, by downregulating activity of signal transduction mechanisms downstream of the EGFR. Numerous studies support cooperation of the Dlg module with vesicle and membrane trafficking, including endocytosis, exocytosis, recycling of endosomes to the cell membrane, and retrograde trafficking (Humbert, 2015; Stephens et al., 2018). In *Drosophila*, Lgl controls endocytosis of the Notch regulator Sanpodo (Roegiers et al., 2005) in sensory precursor cells and attenuates Notch signaling. In eye disc epithelia, Lgl associates with early to late endosomes and lysosomes and attenuates Notch signaling by limiting vesicle acidification (Parsons et al., 2014). Likewise, Scrib optimizes bone morphogenetic protein (BMP) signaling by regulating the basolateral localization of the BMP receptor Thickveins and its internalization in Rab5-positive endosomes in wing epithelia (Gui et al., 2016). In mammalian MDCK (Madin-Darby canine kidney) epithelial cells, Scrib negatively regulates retromer-mediated E-cadherin trafficking to the Golgi (Lohia et al., 2012). Several mechanisms also link the Dlg module to regulation of signal transduction along the EGFR/MAPK pathway (Humbert, 2015; Stephens et al., 2018). For example, human Scrib binds the MAPK/ERK and anchors it to membrane sites to prevent ERK phosphorylation and Ras signaling (Nagasaka et al., 2010). Mammalian Dlg1 binds phosphorylated MEK2, which phosphorylates and activates ERK, to regulate its cortical and perinuclear localization (Gaudet et al., 2011; Maiga et al., 2011), while Dlg2, Dlg3, and Scrib interact with PP1 phosphatases to downregulate ERK phosphorylation (Nagasaka et al., 2013). Presumably, the Dlg module regulates signaling by cooperating with distinct cellular trafficking components in different tissues in part because the availability of partner proteins varies significantly based on cell type and developmental stage.

We also observed that levels of the membrane phospholipid PIP_2 appeared elevated in cyst cells in which function of the Dlg-module or CME components had been knocked

Figure 6. Knockdown of the dPIP5K Kinase *sktl* in Cyst Cells Can Partially Rescue the EGFR Overactivation Phenotypes and Reduce dpERK Levels

Adult testes of the indicated genotypes in the *Gal80^{ts}* background.

(A–H) Vasa (red; germline), TJ (blue; early cyst cell nuclei), *mCD8-GFP* (green; cyst cells), or F-actin stained with phalloidin (green; cyst cells and germline fusome). Small inset pictures show the Vasa staining.

(I–Q) TJ (red) and dpERK (green). Small inset pictures show the dpERK staining.

(R) Quantification of corrected fluorescent dpERK levels in cyst cell (CC) nuclei.

(S) Quantifications of the different phenotypic classes accompanying each genotype, organized in order of phenotypic strength.

Error bars represent standard error. RNAi activated at 30°C for 4 days (d). Testes oriented with anterior at left. Image frames 246 μm (A–H) and 123 μm (I–Q).

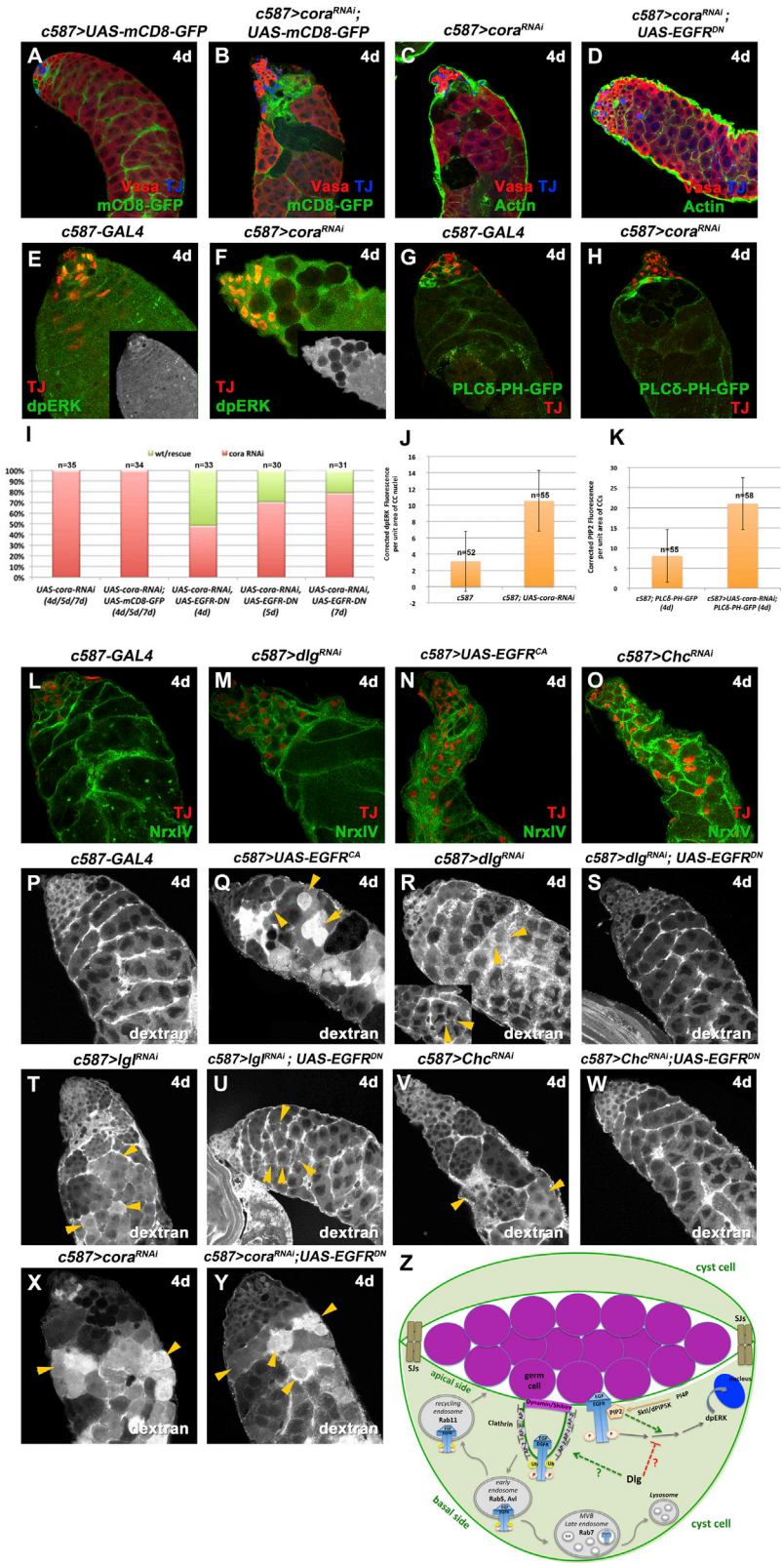

Figure 7. Septate Junction Components Share Common and Distinct Characteristics with the Dlg-Module and CME Components

(A–D) Adult testes of the indicated genotypes in the *Gal80^{ts}* background: Vasa (red; germline), TJ (blue; early cyst cell nuclei), and either *mCD8-GFP* (green; cyst cells) or actin (green; phalloidin marking cyst cells and germline fusome).

(E and F) TJ (red) and dpERK (green). Small inset pictures show the dpERK staining.

(G and H) The PIP_2 reporter PLCδ-PH-GFP expressed in cyst cells (green) and TJ (blue).

(I) Quantification of the different phenotypic classes accompanying each genotype.

(J) Quantification of corrected fluorescent dpERK levels in cyst cell (CC) nuclei depleted.

(K) Quantification of corrected fluorescent PIP_2 levels in early cyst cells (CC) via the PLCδ-PH-GFP reporter.

(L–O) TJ (red) and GFP (green; endogenous NrxIV-GFP).

(P–Y) dextran dye (stained with streptavidin) to test the permeability of the testis barrier. Yellow arrowheads indicate examples of permeability defects.

(Z) Model diagram showing the EGFR signaling pathway and clathrin-mediated EGFR endocytosis in cyst cells, and the possible involvement of the Dlg module and PIP_2. Activation of EGFR at cyst cell membranes activates the Ras/MAPK cascade that leads to dpERK entering the cyst cell nucleus. CME attenuates EGFR signaling by endocytosis of activated EGFR from the membranes. Once in early endosomes, EGFR can either recycle back to the membrane in Rab-11 recycling endosomes or get into multivesicular endosomes (MVE) to be targeted for degradation. Dlg-module components can downregulate EGFR signaling either by cooperating with CME components or by binding and inactivating Ras/MAPK signaling components. PIP_2 binds the EGFR juxtamembrane domain and activates the Ras/MAPK pathway, while Sktl/dPIP5K reduces MAPK activation. SJs from neighboring cyst cells build the testis permeability barrier at cyst cell contact sides, creating an isolated environment for the germ cells they encapsulate.

Error bars represent standard error. RNAi activated at 30°C for 4 days (d). Testes oriented with anterior at left. Image frames, 246 μm (A–D and P–Y) and 123 μm (E–H and L–O). See also Figure S7.

down or when constitutively active EGFR was forcibly expressed, and that loss of function of *Skittles*, the phosphatidylinositol-4-phosphate 5-kinase (PIP5K) that makes PIP_2, partially alleviated those effects, suggesting that the levels of PIP_2 contribute to the phenotype. Membrane PIP_2 is a critical regulator of both membrane trafficking and cell signaling components, including the EGFR (Marat and Haucke, 2016). PIP_2 binds to the EGFR juxtamembrane domain (Abd Halim et al., 2015) and enhances EGFR phosphorylation and activation (Michailidis et al., 2011). Downregulation of PIP_2 levels via pharmacological inhibition or manipulation of PIP5K levels reduces EGFR tyrosine phosphorylation (Michailidis et al., 2011), consistent with our finding of partial rescue by knocking down the function of *Skittles*/PIP5K. It is also possible that EGFR activation promotes the synthesis of PIP_2 by the PIP5K kinase, as enhanced EGFR activity in response to EGF results in increased synthesis of PIP_2 (Funakoshi et al., 2011). Following vesicle endocytosis by CME, maturation of clathrin-coated pits initiates a cascade that locally converts PIP_2 to different phosphatidylinositols and finally to phosphatidylinositol 3-phosphate (PI_3P), an essential feature of early endosomes, in a cascade that is important for vesicle uncoating (Marat and Haucke, 2016; Posor et al., 2015). Blocking early steps of CME by knocking down the function of Shibire AP-2α, or Clathrin heavy chain may thus allow accumulation of higher levels of PIP_2 in cyst cell plasma membranes, where it can promote EGFR activation. Along this line, loss of function of *skittles* rescued the function of cyst cells depleted of Dlg-module and CME components or with increased EGFR signaling, by reducing the levels of phosphorylated MAPK, indicating that the prime output of EGFR affecting cyst cell behavior is MAPK activation, and that the Skittles-PIP_2 equilibrium assists the regulation of MAPK activation in our system.

Dlg, Scrib, Lgl, and CME may partially contribute to the epithelial integrity of the squamous epithelial-like cyst cells but the main regulators seem to be the SJs. Our data show that the Dlg-module and CME components have overlapping but distinct phenotypes with the SJ components. Both Dlg-module and CME components contribute to the maintenance of septate junctions and support the integrity of the testis permeability barrier, yet loss of function of these components in cyst cells does not result in collapse of the barrier function as in the case of core SJ components. Furthermore, lowering the EGFR signaling levels can largely restore the function of the barrier, which is not sufficient in cyst cells depleted of core SJ components. A possible explanation is that loss of the Dlg-module or CME components may affect the polarized distribution of the EGFR, similar to many polarized epithelial cells (Kuwada et al., 1998; Singh and Coffey, 2014), and thus block access of the EGFR to the ligand Spitz secreted by the germ cells and thereby attenuate the EGFR signaling.

Our results uncover regulatory strategies on how endocytosis and polarity cues cooperate with signaling to coordinate stem cell maintenance versus differentiation and sculpt developing tissues. The high degree of conservation of these components across species allows us to extend the basic mechanistic features of cell-cell communication uncovered here to other tissues and organisms.

EXPERIMENTAL PROCEDURES

Fly Stocks and Husbandry

Fly stocks used in this study are described in FlyBase (www.flybase.org). Fly stocks are listed in Supplemental Experimental Procedures. All *UAS-gene^{RNAi}* stocks are referred to in the text as *gene^{RNAi}*. Crosses were raised at 18°C until adult flies hatched. Males with the correct genotype were then shifted at 30°C for 2–7 days depending on the experimental needs, and the phenotypes were analyzed.

Immunofluorescence Staining and Microscopy

Immunostaining of whole-mount testes was performed as previously described (Papagiannouli and Mechler, 2009). For testes immunostaining in the presence of GFP, 1% PBT (1% Tween 20 in PBS) was used instead of 1% PBX in all steps. For the TUNEL assay the In Situ Cell Death Detection Kit (TMR Red, Sigma/Roche), protocol was followed immediately after fixation. A detailed staining protocol and list of antibodies can be found in Supplemental Experimental Procedures.

Confocal images were obtained using a Leica SP8 system. Pictures were processed with Adobe Photoshop 7.0. Quantifications were done using FiJi/ImageJ by measuring "Corrected Total Cell Fluorescence."

SUPPLEMENTAL INFORMATION

Supplemental Information can be found online at https://doi.org/10.1016/j.stemcr.2019.03.008.

AUTHOR CONTRIBUTIONS

F.P. designed, performed, and interpreted experiments, wrote the paper, and obtained funding to support the study. C.W.B. did preliminary work on EGFR. M.T.F. co-designed and interpreted experiments, assisted with writing the paper, and obtained funding to support the study.

ACKNOWLEDGMENTS

We thank Jaclyn Lim and Susanna Brantley for preliminary data, experiment interpretation, and helpful discussions. We thank the generous *Drosophila* community for fly stocks and antibodies, in particular Dorothea Godt, Ruth Lehmann, Antoine Guichet, Dennis McKearin, DSHB, VDRC, and BDSC Centers. We deeply thank Maria Leptin, as part of this work was done in her lab. This work was supported by the DFG PA2659/4-1 and 5-1 to F.P.

and NIH grant 1 R01 GM080501 to M.T.F. We thank the Cell Sciences Imaging Facility (Beckmann Center, Stanford University) and CECAD Imaging Facility (University of Cologne) for technical support.

Received: August 23, 2018
Revised: March 21, 2019
Accepted: March 22, 2019
Published: April 18, 2019

REFERENCES

Abd Halim, K.B., Koldso, H., and Sansom, M.S.P. (2015). Interactions of the EGFR juxtamembrane domain with PIP2-containing lipid bilayers: insights from multiscale molecular dynamics simulations. Biochim. Biophys. Acta *1850*, 1017–1025.

Balakrishnan, S.S., Basu, U., and Raghu, P. (2015). Phosphoinositide signalling in *Drosophila*. Biochim. Biophys. Acta *1851*, 770–784.

Bilder, D., and Perrimon, N. (2000). Localization of apical epithelial determinants by the basolateral PDZ protein Scribble. Nature *403*, 676–680.

Chen, M.L., Green, D., Liu, L., Lam, Y.C., Mukai, L., Rao, S., Ramagiri, S., Krishnan, K.S., Engel, J.E., Lin, J.J., et al. (2002). Unique biochemical and behavioral alterations in *Drosophila* shibire(ts1) mutants imply a conformational state affecting dynamin subcellular distribution and synaptic vesicle cycling. J. Neurobiol. *53*, 319–329.

Conte, A., and Sigismund, S. (2016). Chapter Six—The ubiquitin network in the control of EGFR endocytosis and signaling. Prog. Mol. Biol. Transl. Sci. *141*, 225–276.

Czech, M.P. (2000). PIP2 and PIP3: complex roles at the cell surface. Cell *100*, 603–606.

de Vreede, G., Schoenfeld, J.D., Windler, S.L., Morrison, H., Lu, H., and Bilder, D. (2014). The Scribble module regulates retromer-dependent endocytic trafficking during epithelial polarization. Development *141*, 2796–2802.

Donohoe, C.D., Csordas, G., Correia, A., Jindra, M., Klein, C., Habermann, B., and Uhlirova, M. (2018). Atf3 links loss of epithelial polarity to defects in cell differentiation and cytoarchitecture. PLoS Genet. *14*, e1007241.

Fairchild, M.J., Islam, F., and Tanentzapf, G. (2017). Identification of genetic networks that act in the somatic cells of the testis to mediate the developmental program of spermatogenesis. PLoS Genet. *13*, e1007026.

Fairchild, M.J., Smendziuk, C.M., and Tanentzapf, G. (2015). A somatic permeability barrier around the germline is essential for *Drosophila* spermatogenesis. Development *142*, 268–281.

Fehon, R.G., Dawson, I.A., and Artavanis-Tsakonas, S. (1994). A *Drosophila* homologue of membrane-skeleton protein 4.1 is associated with septate junctions and is encoded by the coracle gene. Development *120*, 545–557.

Fuller, M.T., and Spradling, A.C. (2007). Male and female *Drosophila* germline stem cells: two versions of immortality. Science *316*, 402–404.

Funakoshi, Y., Hasegawa, H., and Kanaho, Y. (2011). Regulation of PIP5K activity by Arf6 and its physiological significance. J. Cell Physiol. *226*, 888–895.

Gaudet, S., Langlois, M.J., Lue, R.A., Rivard, N., and Viel, A. (2011). The MEK2-binding tumor suppressor hDlg is recruited by E-cadherin to the midbody ring. BMC Cell Biol. *12*, 55.

Gervais, L., Claret, S., Januschke, J., Roth, S., and Guichet, A. (2008). PIP5K-dependent production of PIP2 sustains microtubule organization to establish polarized transport in the *Drosophila* oocyte. Development *135*, 3829–3838.

Goh, L.K., and Sorkin, A. (2013). Endocytosis of receptor tyrosine kinases. Cold Spring Harb. Perspect. Biol. *5*, a017459.

Gonczy, P., and DiNardo, S. (1996). The germ line regulates somatic cyst cell proliferation and fate during *Drosophila* spermatogenesis. Development *122*, 2437–2447.

Goode, S., and Perrimon, N. (1997). Inhibition of patterned cell shape change and cell invasion by Discs large during *Drosophila* oogenesis. Genes Dev. *11*, 2532–2544.

Gui, J., Huang, Y., and Shimmi, O. (2016). Scribbled optimizes BMP signaling through its receptor internalization to the Rab5 endosome and promote robust epithelial morphogenesis. PLoS Genet. *12*, e1006424.

Hudson, A.G., Parrott, B.B., Qian, Y., and Schulz, C. (2013). A temporal signature of epidermal growth factor signaling regulates the differentiation of germline cells in testes of *Drosophila melanogaster*. PLoS One *8*, e70678.

Humbert, P.O.R., Russell, S.M., Smith, L., and Richardson, H.E. (2015). The Scribble-Dlg-Lgl module in cell polarity regulation. In Cell Polarity 1, K. Ebnet, ed. (Springer International Publishing), pp. 65–111.

Kiger, A.A., White-Cooper, H., and Fuller, M.T. (2000). Somatic support cells restrict germline stem cell self-renewal and promote differentiation. Nature *407*, 750–754.

Kuwada, S.K., Lund, K.A., Li, X.F., Cliften, P., Amsler, K., Opresko, L.K., and Wiley, H.S. (1998). Differential signaling and regulation of apical vs. basolateral EGFR in polarized epithelial cells. Am. J. Physiol. *275*, C1419–C1428.

Leatherman, J. (2013). Stem cells supporting other stem cells. Front. Genet. *4*, 257.

Leatherman, J.L., and Dinardo, S. (2008). Zfh-1 controls somatic stem cell self-renewal in the *Drosophila* testis and nonautonomously influences germline stem cell self-renewal. Cell Stem Cell *3*, 44–54.

Li, M., Marhold, J., Gatos, A., Torok, I., and Mechler, B.M. (2001). Differential expression of two scribble isoforms during *Drosophila* embryogenesis. Mech. Dev. *108*, 185–190.

Lim, J.G., and Fuller, M.T. (2012). Somatic cell lineage is required for differentiation and not maintenance of germline stem cells in *Drosophila* testes. Proc. Natl. Acad. Sci. U S A *109*, 18477–18481.

Lohia, M., Qin, Y., and Macara, I.G. (2012). The Scribble polarity protein stabilizes E-cadherin/p120-catenin binding and blocks retrieval of E-cadherin to the Golgi. PLoS One *7*, e51130.

Losick, V.P., Morris, L.X., Fox, D.T., and Spradling, A. (2011). *Drosophila* stem cell niches: a decade of discovery suggests a unified view of stem cell regulation. Dev. Cell *21*, 159–171.

Maiga, O., Philippe, M., Kotelevets, L., Chastre, E., Benadda, S., Pidard, D., Vranckx, R., and Walch, L. (2011). Identification of mitogen-activated protein/extracellular signal-responsive kinase kinase 2 as a novel partner of the scaffolding protein human homolog of disc-large. FEBS J. *278*, 2655–2665.

Marat, A.L., and Haucke, V. (2016). Phosphatidylinositol 3-phosphates-at the interface between cell signalling and membrane traffic. EMBO J. *35*, 561–579.

Marhold, J., Papagiannouli, F., Li, M., Patel, A., and Mechler, B.M. (2003). Requirements for scribble expression in newly formed gonads of *Drosophila* embryos. Gene Expr. Patterns *3*, 143–146.

Matunis, E.L., Stine, R.R., and de Cuevas, M. (2012). Recent advances in *Drosophila* male germline stem cell biology. Spermatogenesis *2*, 137–144.

Michailidis, I.E., Rusinova, R., Georgakopoulos, A., Chen, Y., Iyengar, R., Robakis, N.K., Logothetis, D.E., and Baki, L. (2011). Phosphatidylinositol-4,5-bisphosphate regulates epidermal growth factor receptor activation. Pflugers Arch. *461*, 387–397.

Monahan, A.J., and Starz-Gaiano, M. (2016). Apontic regulates somatic stem cell numbers in *Drosophila* testes. BMC Dev. Biol. *16*, 5.

Nagasaka, K., Pim, D., Massimi, P., Thomas, M., Tomaic, V., Subbaiah, V.K., Kranjec, C., Nakagawa, S., Yano, T., Taketani, Y., et al. (2010). The cell polarity regulator hScrib controls ERK activation through a KIM site-dependent interaction. Oncogene *29*, 5311–5321.

Nagasaka, K., Seiki, T., Yamashita, A., Massimi, P., Subbaiah, V.K., Thomas, M., Kranjec, C., Kawana, K., Nakagawa, S., Yano, T., et al. (2013). A novel interaction between hScrib and PP1gamma downregulates ERK signaling and suppresses oncogene-induced cell transformation. PLoS One *8*, e53752.

Oshima, K., and Fehon, R.G. (2011). Analysis of protein dynamics within the septate junction reveals a highly stable core protein complex that does not include the basolateral polarity protein Discs large. J. Cell Sci. *124*, 2861–2871.

Papagiannouli, F. (2013). The internal structure of embryonic gonads and testis development in *Drosophila melanogaster* requires scrib, lgl and dlg activity in the soma. Int. J. Dev. Biol. *57*, 25–34.

Papagiannouli, F., and Lohmann, I. (2012). Shaping the niche: Lessons from the *Drosophila* testis and other model systems. Biotechnol. J. *7*, 723–736.

Papagiannouli, F., and Mechler, B.M. (2009). Discs large regulates somatic cyst cell survival and expansion in *Drosophila* testis. Cell Res. *19*, 1139–1149.

Parsons, L.M., Portela, M., Grzeschik, N.A., and Richardson, H.E. (2014). Lgl regulates Notch signaling via endocytosis, independently of the apical aPKC-Par6-Baz polarity complex. Curr. Biol. *24*, 2073–2084.

Posor, Y., Eichhorn-Grunig, M., and Haucke, V. (2015). Phosphoinositides in endocytosis. Biochim. Biophys. Acta *1851*, 794–804.

Roegiers, F., Jan, L.Y., and Jan, Y.N. (2005). Regulation of membrane localization of Sanpodo by lethal giant larvae and neuralized in asymmetrically dividing cells of *Drosophila* sensory organs. Mol. Biol. Cell *16*, 3480–3487.

Sarkar, A., Parikh, N., Hearn, S.A., Fuller, M.T., Tazuke, S.I., and Schulz, C. (2007). Antagonistic roles of Rac and Rho in organizing the germ cell microenvironment. Curr. Biol. *17*, 1253–1258.

Schulz, C., Wood, C.G., Jones, D.L., Tazuke, S.I., and Fuller, M.T. (2002). Signaling from germ cells mediated by the rhomboid homolog stet organizes encapsulation by somatic support cells. Development *129*, 4523–4534.

Singh, B., and Coffey, R.J. (2014). Trafficking of epidermal growth factor receptor ligands in polarized epithelial cells. Annu. Rev. Physiol. *76*, 275–300.

Singh, S.R., Liu, Y., Zhao, J., Zeng, X., and Hou, S.X. (2016). The novel tumour suppressor Madm regulates stem cell competition in the *Drosophila* testis. Nat. Commun. *7*, 10473.

Stephens, R., Lim, K., Portela, M., Kvansakul, M., Humbert, P.O., and Richardson, H.E. (2018). The scribble cell polarity module in the regulation of cell signaling in tissue development and tumorigenesis. J. Mol. Biol. *430*, 3585–3612.

Tran, J., Brenner, T.J., and DiNardo, S. (2000). Somatic control over the germline stem cell lineage during *Drosophila* spermatogenesis. Nature *407*, 754–757.

Uhlirova, M., and Bohmann, D. (2006). JNK- and Fos-regulated Mmp1 expression cooperates with Ras to induce invasive tumors in *Drosophila*. EMBO J. *25*, 5294–5304.

Woods, D.F., Hough, C., Peel, D., Callaini, G., and Bryant, P.J. (1996). Dlg protein is required for junction structure, cell polarity, and proliferation control in *Drosophila* epithelia. J. Cell Biol. *134*, 1469–1482.

Zoller, R., and Schulz, C. (2012). The *Drosophila* cyst stem cell lineage: partners behind the scenes? Spermatogenesis *2*, 145–157.

Stem Cell Reports, Volume *12*

Supplemental Information

The Dlg Module and Clathrin-Mediated Endocytosis Regulate EGFR Signaling and Cyst Cell-Germline Coordination in the *Drosophila* Testis

Fani Papagiannouli, Cameron Wynn Berry, and Margaret T. Fuller

Supplemental Information

The Dlg-module and clathrin-mediated endocytosis regulate EGFR signaling and cyst cell-germline coordination in the *Drosophila* testis.

Fani Papagiannouli, Cameron Wynn Berry, Margaret T. Fuller

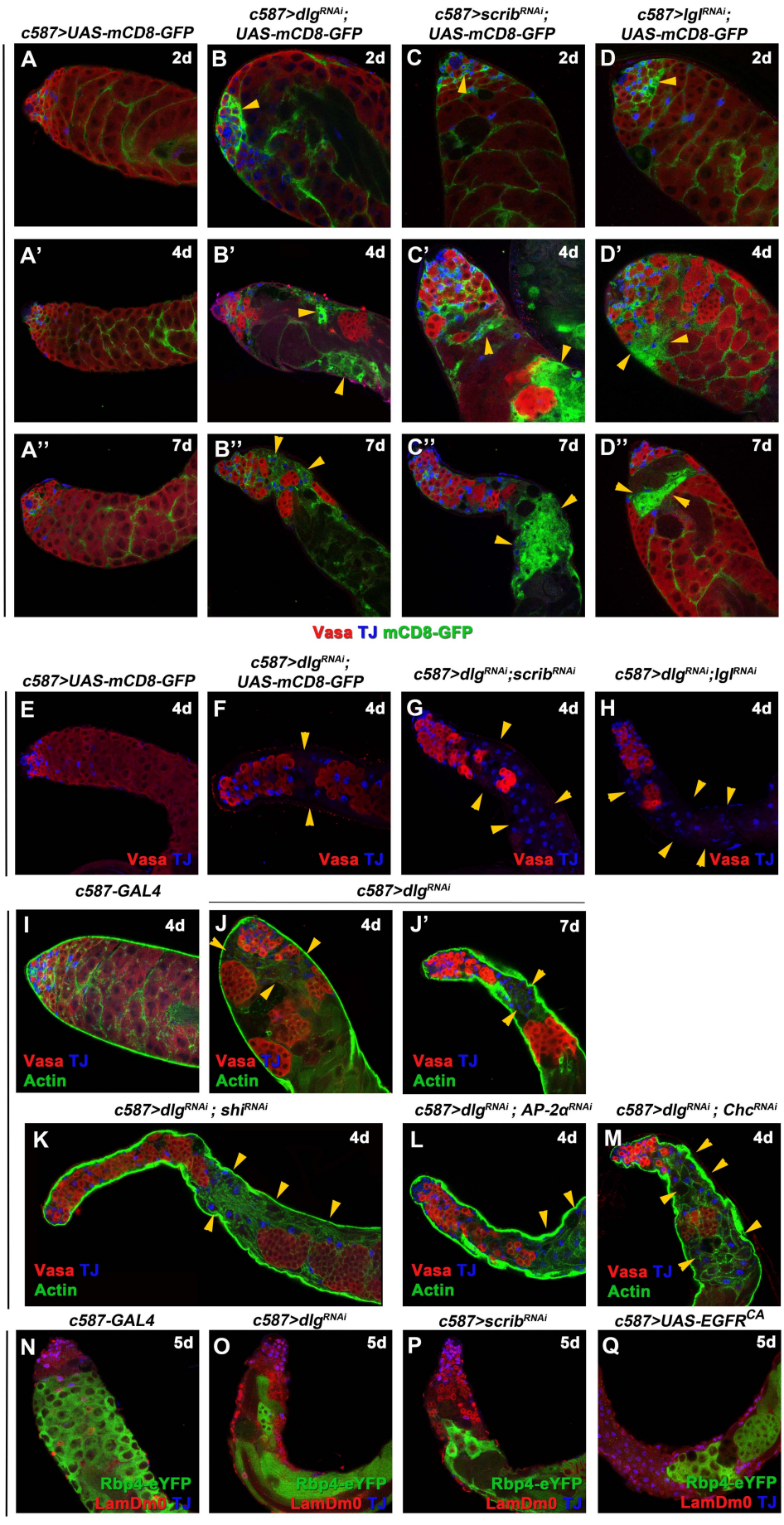
c587>UAS-mCD8-GFP
c587>dlg^RNAi; UAS-mCD8-GFP
c587>scrib^RNAi; UAS-mCD8-GFP
c587>lgl^RNAi; UAS-mCD8-GFP
A 2d
B 2d
C 2d
D 2d
A' 4d
B' 4d
C' 4d
D' 4d
A'' 7d
B'' 7d
C'' 7d
D'' 7d
Vasa TJ mCD8-GFP
c587>UAS-mCD8-GFP
c587>dlg^RNAi; UAS-mCD8-GFP
c587>dlg^RNAi;scrib^RNAi
c587>dlg^RNAi;lgl^RNAi
E 4d
F 4d
G 4d
H 4d
Vasa TJ
c587-GAL4
c587>dlg^RNAi
I 4d
J 4d
J' 7d
Vasa TJ Actin
c587>dlg^RNAi ; shi^RNAi
c587>dlg^RNAi ; AP-2α^RNAi
c587>dlg^RNAi ; Chc^RNAi
K 4d
L 4d
M 4d
c587-GAL4
c587>dlg^RNAi
c587>scrib^RNAi
c587>UAS-EGFR^CA
N 5d
O 5d
P 5d
Q 5d
Rbp4-eYFP LamDm0 TJ

Figure S1: Knockdown *dlg*, *scrib*, *lgl* or clathrin-mediate endocytosis in cyst cells leads to cell non-autonomous germ cell death and comparable defects in double knockdown combinations. Related to Fig. 1 and 4. Adult testes of the indicated genotypes in the background of the *Gal80^{ts}* **(A-D'')** *mCD8-GFP* (green) expressed in cyst cells; anti-Vasa (red; germline); anti-TJ (blue; early cyst cell nuclei). Yellow arrowheads: mCD8-positive cyst cell regions. **(E-H)** immunostainings with anti-Vasa (red) and anti-TJ (blue). **(I-M)** immunostainings with anti-Vasa (red; germline), anti-TJ (blue; early cyst cell nuclei) and F-actin stained for phalloidin (green; cyst cells and germline fusome). **(N-Q)** immunostainings with anti-LamDm0 (red), anti-TJ (blue) and anti-GFP (green) for Rbp4-positive spermatocytes. Yellow arrowheads indicate cyst cell clusters. Newly eclosed male flies were shifted at 30^{o}C to activate the RNAi for 2, 4 and 7 days (d). Testes oriented with anterior at left. Image frame 246µm.

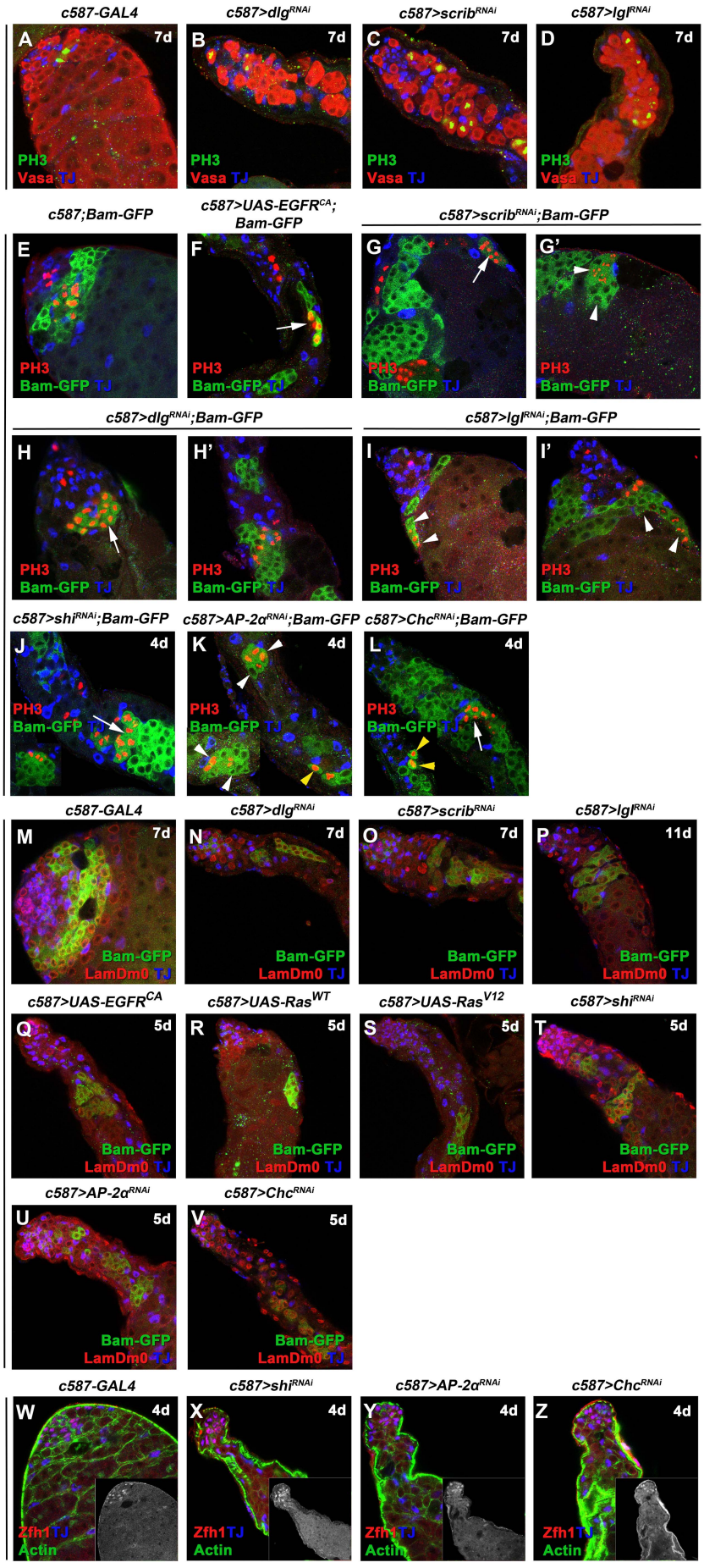
c587-GAL4
c587>dlg^RNAi
c587>scrib^RNAi
c587>lgl^RNAi
A 7d
B 7d
C 7d
D 7d
PH3
Vasa TJ
c587;Bam-GFP
c587>UAS-EGFR^CA; Bam-GFP
c587>scrib^RNAi;Bam-GFP
E
F
G
G'
PH3
Bam-GFP TJ
c587>dlg^RNAi;Bam-GFP
c587>lgl^RNAi;Bam-GFP
H
H'
I
I'
c587>shi^RNAi;Bam-GFP
c587>AP-2α^RNAi;Bam-GFP
c587>Chc^RNAi;Bam-GFP
J 4d
K 4d
L 4d
c587-GAL4
c587>dlg^RNAi
c587>scrib^RNAi
c587>lgl^RNAi
M 7d
N 7d
O 7d
P 11d
Bam-GFP
LamDm0 TJ
c587>UAS-EGFR^CA
c587>UAS-Ras^WT
c587>UAS-Ras^V12
c587>shi^RNAi
Q 5d
R 5d
S 5d
T 5d
c587>AP-2α^RNAi
c587>Chc^RNAi
U 5d
V 5d
c587-GAL4
c587>shi^RNAi
c587>AP-2α^RNAi
c587>Chc^RNAi
W 4d
X 4d
Y 4d
Z 4d
Zfh1 TJ
Actin

Figure S2: Knockdown of *dlg, scrib, lgl* and CME components or EGFR overactivation in cyst cells results in similar non-autonomous loss of spermatogonia and spermatocytes, while remaining germ cells retain their proliferation capacity. **Related to Fig. 1, 2 and 4**. Adult testes of the indicated genotypes in the background of the *Gal80^{ts}*. **(A-D)** immunostainings with anti-Vasa (red; germline), anti-TJ (blue; early cyst cell nuclei) and anti-PH3 (green) marking cells in mitosis. **(E-L)** Bam-GFP transgene (red) expressed in late spermatogonia, anti-TJ (blue; early cyst cell nuclei) and anti-PH3 (green) marking cells in mitosis. Arrows point at Bam-positive spermatogonial cysts that divide synchronously. White arrowheads point at Bam-positive spermatogonial cysts that divide asynchronously as not all germ cells within each cyst are PH3 positive. Yellow arrowheads point at Bam-positive spermatogonia. **(M-V)** Bam-GFP transgene (green) in late spermatogonia, anti-LamDm0 (red) marking cyst cells and early germ cells (GSCs, GBs and spermatogonia), anti-TJ (blue; early cyst cell nuclei). (A'-J') higher magnifications of testes apical region. **(W-Z)** immunostainings with anti-Zfh1 (red; CySCs and daughters), anti-TJ (blue) and Phalloidin (green; F-actin). Small inset pictures show the Zfh-1 panels from (W-Z). Testes oriented with anterior at left. Image frame (A-V) 123μm, (W-Z) 246μm.

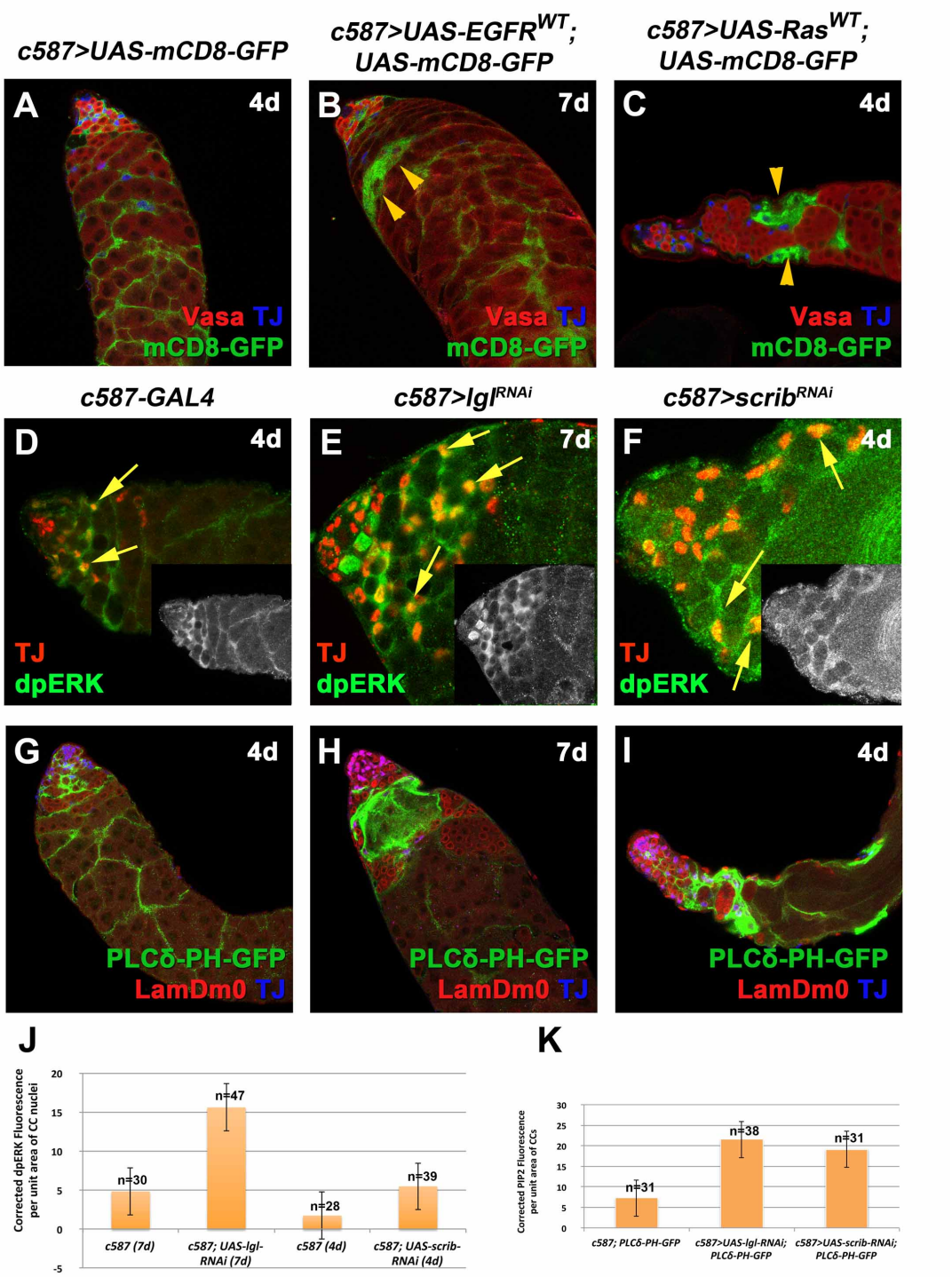

Figure S3: Knockdown of *scrib* and *lgl* or overactivation of EGFR receptor signaling in cyst cells have similar phenotypes. Related to Fig. 2. (A-C) *mCD8-GFP* (green) expressed in cyst cells; anti-Vasa (red; germline) and anti-TJ (blue; early cyst cell nuclei). **(D-F)** anti-TJ (red) and anti-dpERK (green). Yellow arrows: examples of cyst cells double-labeled for TJ and dpERK. Small inset pictures show the anti-dpERK staining only. **(G-I)** the PIP2 reporter PLCδ-PH-GFP expressed in cyst cells (green), anti-LamDm0 (red) marking cyst cells and early germ cells (GSCs, GBs and spermatogonia), anti-TJ (blue; early cyst cell nuclei). **(J)** Quantification of corrected fluorescent dpERK levels in cyst cell (CC) nuclei depleted of *scrib* and *lgl* function. **(K)** Quantification of corrected fluorescent PIP2 levels in cyst cells (CC) via the PLCδ-PH-GFP reporter. Testes oriented with anterior at left. Image frame (A-C, G-I) 246µm, (D-F) 123µm.

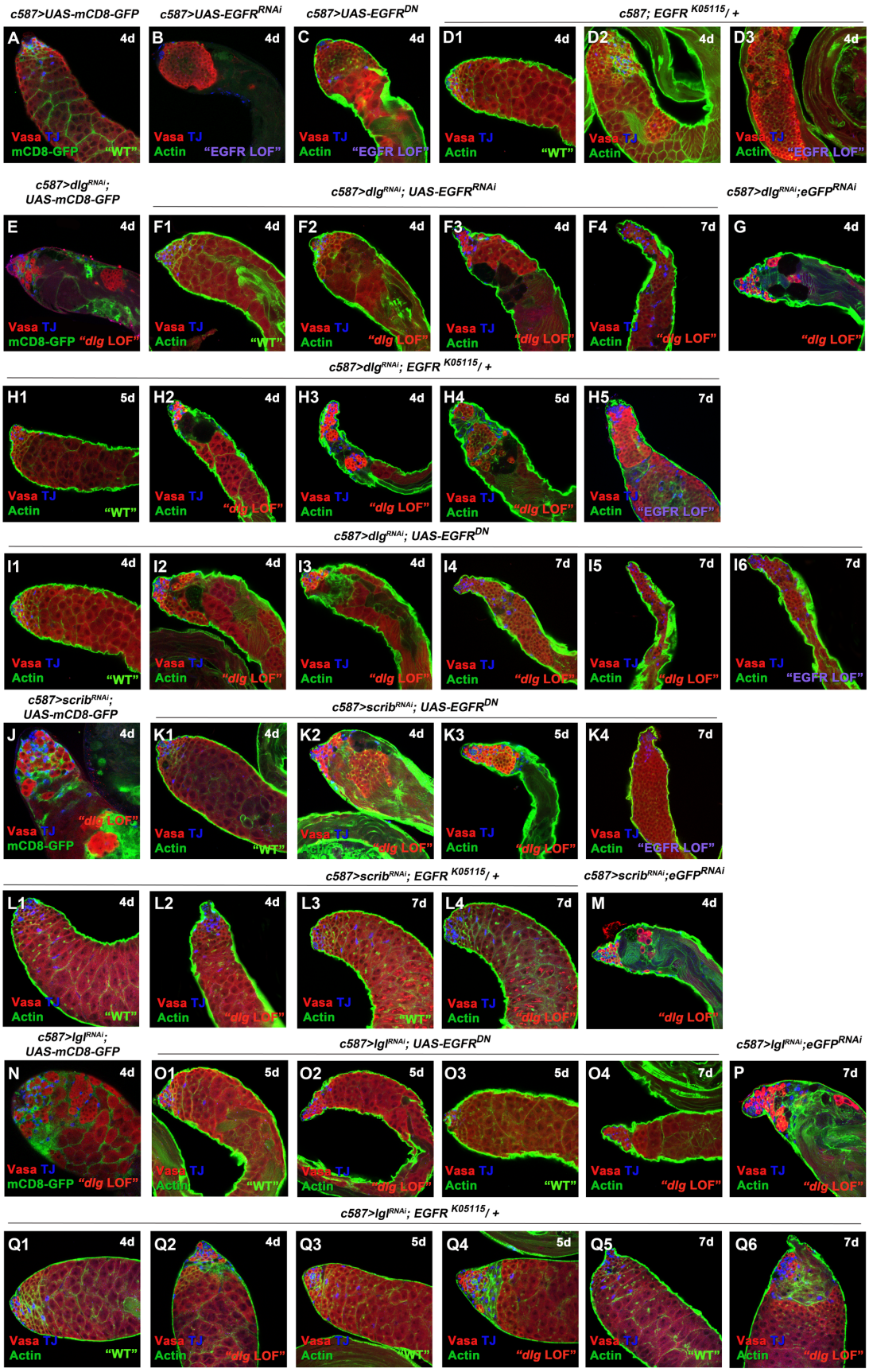

Figure S4: Lowering EGFR signaling levels can rescue the *dlg*, *scrib* and *lgl* loss of function phenotypes in adult testis. Related to Fig. 3. Adult testes of the indicated genotypes in the background of the *Gal80^{ts}*. Testes immunostained with anti-Vasa (red; germline), anti-TJ (blue; early cyst cell nuclei) and either anti-GFP (green) for the *mCD8-GFP* expressed in cyst cells or Phalloidin

(green; F-actin in cyst cells and germline fusome) depending on the genotype. Representative pictures for each genotype used, and the phenotypic classes accompanying them are shown. Order of phenotypic strength: weak and strong "dlg LOF", "wt" and "EGFR LOF". Newly eclosed male flies were shifted at 30^{o}C to activate the RNAi for 4, 5 and 7 days. Testes oriented with anterior at left. Image frame 246μm.

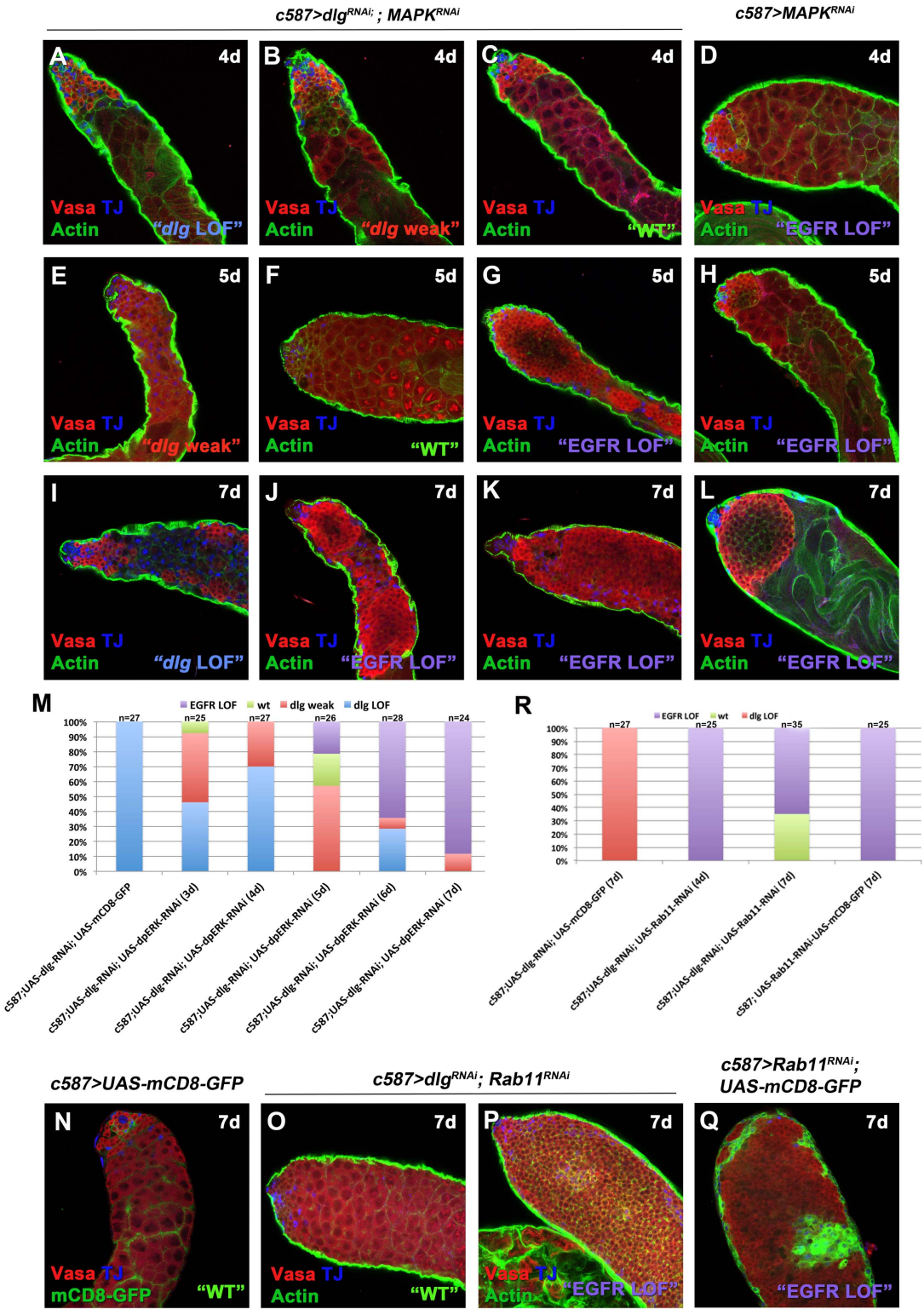

Figure S5: Lowering EGFR signaling levels by knocking down the MAPK or recycling endosome component Rab11 in cyst cells can rescue the *dlg* defects in cyst cells. Related to Fig. 3 and 5. Adult testes of the indicated genotypes in the background of the *Gal80*^{ts}. Newly eclosed male flies were shifted at 30^{o}C to activate the RNAi for 4, 5 and 7 days. **(A-M) Knockdown of MAPK in cyst cells. (A-L)** F-actin stained for phalloidin (green; cyst cells and germline fusome); anti-Vasa (red); anti-TJ (blue). Double-knockdown of MAPK and *dlg* by RNAi in cyst cells for 3-5 days resulted in partially rescued weak *dlg* phenotypes (Fig.S6B, S6E) or even resembled the wild type controls (Fig.S6C). In double-knockdowns for 6-7 days, less than 30% of the testes scored showed the "dlg LOF" phenotype and the majority of testes fell in the "EGFR LOF" class (Fig. S6K, S6M). **(M)** Quantifications of the

different phenotypic classes accompanying each genotype, organized in order of phenotypic strength: “dlg LOF”, “dlg weak”, “wt” and “EGFR LOF”. **(N-R) Knockdown of Rab11 in cyst cells. (N, Q)** *mCD8-GFP* (green) expressed in cyst cells; anti-Vasa (red; germline); anti-TJ (blue; early cyst cell nuclei), **(O, P)** F-actin stained for phalloidin (green; cyst cells and germline fusome); anti-Vasa (red); anti-TJ (blue). **(R)** Quantifications of the different phenotypic classes accompanying each genotype, organized in order of phenotypic strength: “dlg LOF”, “wt” and “EGFR LOF”. Testes oriented with anterior at left. Image frame 246μm.

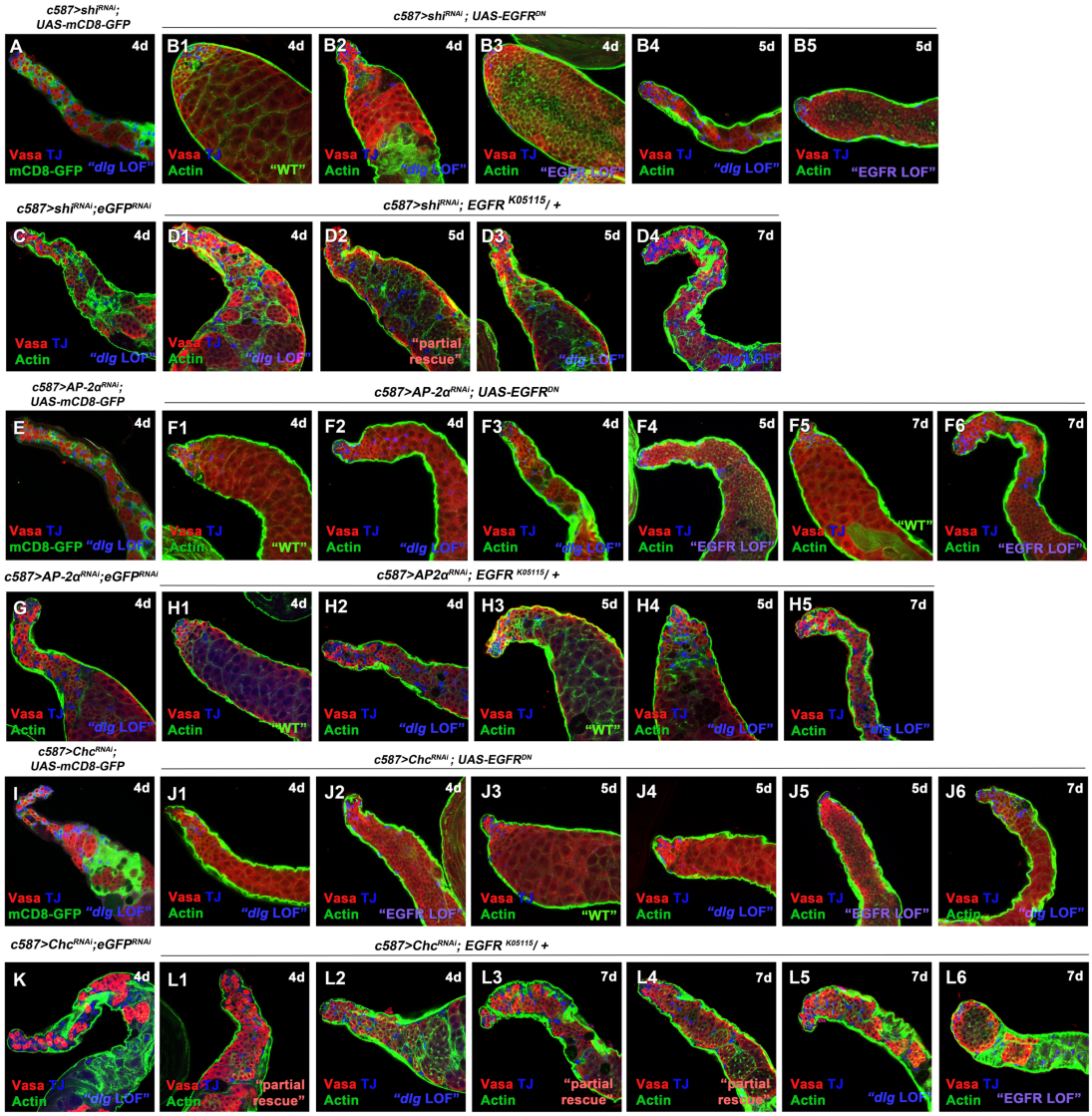

Figure S6: Lowering EGFR signaling levels can rescue the *shi, AP-2α* or *Chc* knockdown phenotypes in cyst cells. **Related to Fig. 5.** Adult testes of the indicated genotypes in the background of the *Gal80^{ts}* immunostained with anti-Vasa (red; germline), anti-TJ (blue; early cyst cell nuclei) and either anti-GFP (green) for the *mCD8-GFP* or Phalloidin (green; F-actin marking cyst cells and germline fusome), depending on the genotype. Representative pictures for each genotype used and the phenotypic classes accompanying them are shown. Order of phenotypic strength: "dlg LOF", "partial rescue", "wt" and "EGFR LOF". Newly eclosed male flies were shifted at 30^{o}C to activate the RNAi for 4, 5 and 7 days. Testes oriented with anterior at left. Image frame 246μm.

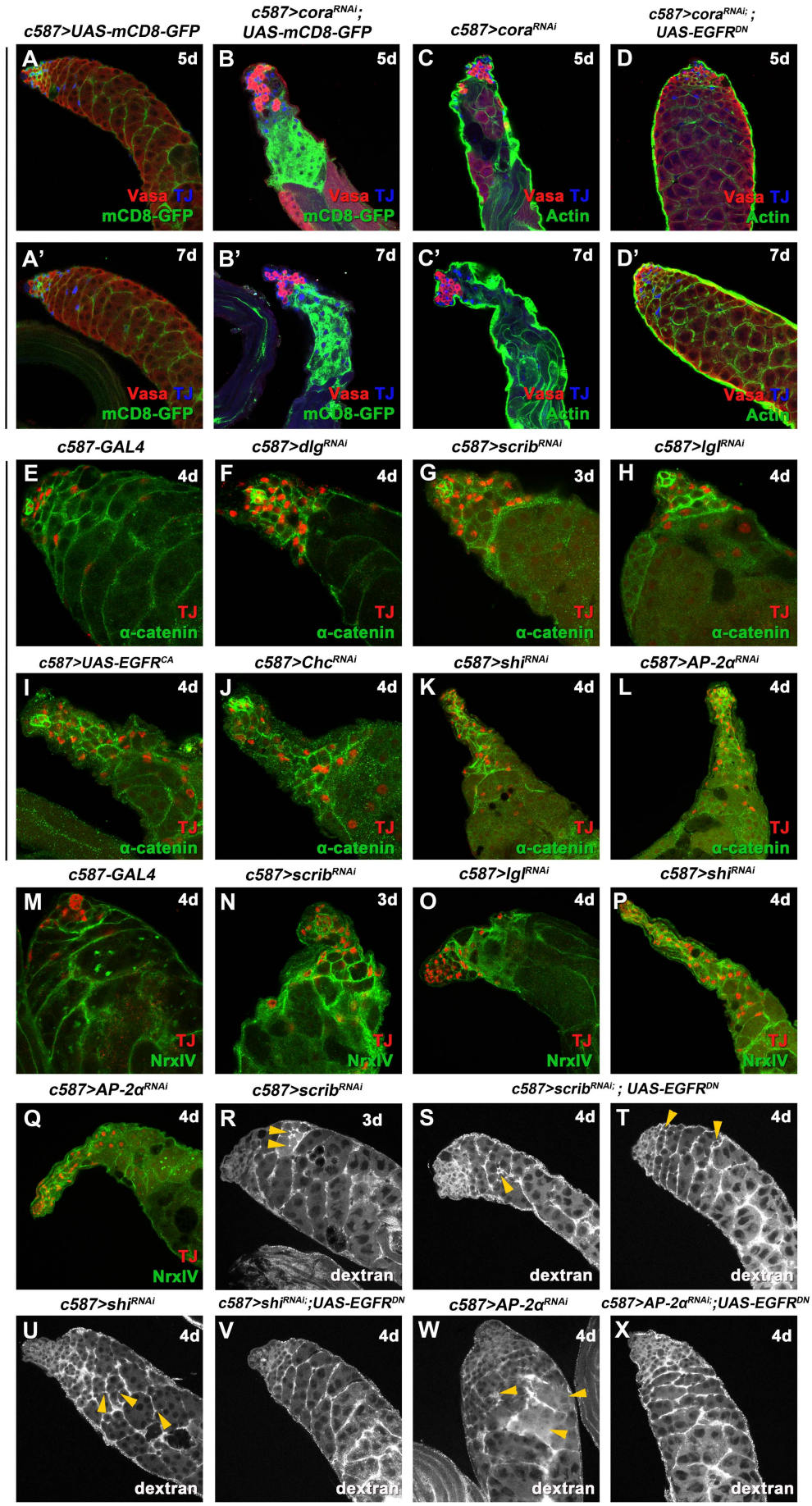
c587>UAS-mCD8-GFP
c587>cora^RNAi; UAS-mCD8-GFP
c587>cora^RNAi
c587>cora^RNAi; UAS-EGFR^DN
A 5d Vasa TJ mCD8-GFP
B 5d Vasa TJ mCD8-GFP
C 5d Vasa TJ Actin
D 5d Vasa TJ Actin
A' 7d Vasa TJ mCD8-GFP
B' 7d Vasa TJ mCD8-GFP
C' 7d Vasa TJ Actin
D' 7d Vasa TJ Actin
c587-GAL4
c587>dlg^RNAi
c587>scrib^RNAi
c587>lgl^RNAi
E 4d TJ α-catenin
F 4d TJ α-catenin
G 3d TJ α-catenin
H 4d TJ α-catenin
c587>UAS-EGFR^CA
c587>Chc^RNAi
c587>shi^RNAi
c587>AP-2α^RNAi
I 4d TJ α-catenin
J 4d TJ α-catenin
K 4d TJ α-catenin
L 4d TJ α-catenin
c587-GAL4
c587>scrib^RNAi
c587>lgl^RNAi
c587>shi^RNAi
M 4d TJ NrxIV
N 3d TJ NrxIV
O 4d TJ NrxIV
P 4d TJ NrxIV
c587>AP-2α^RNAi
c587>scrib^RNAi
c587>scrib^RNAi; UAS-EGFR^DN
Q 4d TJ NrxIV
R 3d dextran
S 4d dextran
T 4d dextran
c587>shi^RNAi
c587>shi^RNAi;UAS-EGFR^DN
c587>AP-2α^RNAi
c587>AP-2α^RNAi;UAS-EGFR^DN
U 4d dextran
V 4d dextran
W 4d dextran
X 4d dextran

Figure S7: Septate junction components share common and distinct characteristics to the Dlg-module and CME components. **Related to Fig. 7.** Adult testes of the indicated genotypes in the background of the *Gal80^{ts}*: **(A-D')** immunostained with anti-Vasa (red; germline), anti-TJ (blue; early cyst cell nuclei) and either anti-GFP (green) for the *mCD8-GFP* or Phalloidin (green; F-actin marking cyst cells and germline fusome), depending on the genotype, **(E-L)** stained with anti-TJ (red) and anti-GFP (green) for the endogenous α-Catenin-YFP, **(M-Q)** stained with anti-TJ (red) and anti-GFP (green) for the endogenous NrxIV-GFP, **(R-X)** dextran dye stained with streptavidin, showing that the dye can access late spermatogonia and spermatocytes when the permeability of testis barrier is compromised or defective. Yellow arrowheads point at examples of permeability defects. Newly eclosed male flies were shifted at 30^{o}C to activate the RNAi for 4, 5 and 7 days, as indicated. Testes oriented with anterior at left. Image frame (A-D', R-X) 246μm, (E-Q) 123μm.

SUPPLEMENTAL EXPERIMENTAL PROCEDURES

Fly stocks and husbandry

The following stocks were obtained from the Bloomington Stock Center (BL) Indiana: *UAS-sktl-RNAi$^{TRiP.JF02796}$*, *UAS-sktl-RNAi$^{TRiP.GL00072}$*, *UAS-ERK-RNAi$^{TRiP.HMS00173}$*, *UAS-scrib-RNAi$^{TRiP.HMS01490}$*, *UAS-AP2α (adaptin)-RNAi$^{TRiP.HMS00653}$*, *UAS-shi-RNAi$^{TRiP.JF03133}$*, *UAS-EGFR-RNAi$^{TRiP.HMS05003}$*, *UAS-sktl-RNAi$^{TRiP.JF02796}$* (BL27715), *UAS-sktl-RNAi$^{TRiP.GL00072}$* (BL35198), *UAS-EGFR^{DN}* (BL5364), *UAS-EGFR^{CA}* (BL9533), *UAS-EGFR^{WT}* (BL5368), *UAS-shi^{ts1}* (BL44222), *UAS-Ras85D^{V12}* (BL4847), *UAS-mCD8-GFP* (BL5139), *Pin/CyO; UAS-mCD8-GFP* (BL5130), *PLCδ-PH-GFP* (BL57353), *P{lacW}EGFR^{K05115}/CyO* (BL10385), *αtub84B-GAL80^{ts}/TM2* (BL7017), *tub-GAL80^{ts}; TM2/TM6B,Tb* (BL7019), *lgl-GAL4^{GMR27F03}* (BL47341) (Papagiannouli, 2013). The following stocks used in this study were obtained from the Vienna *Drosophila* RNAi Center (VDRC) Austria: *UAS-dlg-RNAi^{v41134}, UAS-dlg-RNAi^{v41136}/TM3, UAS-lgl-RNAi^{v109604}, UAS-lgl-RNAi^{v51247}, UAS-Chc-RNAi^{v103383} , UAS-Chc-RNAi^{v32666} , UAS-EGFR-RNAi^{v43267} , UAS-Ras85D-RNAi^{v28129} UAS-Rab11-RNAi^{v22198}, UAS-Rab11-RNAi^{v108382}, UAS-cora-RNAi^{v9787}*. The *scrib-GFP^{CA07683}* and *NrxIV-GFP^{CA06597}* were obtained from Spradling [GFP project; (Buszczak et al., 2007; Papagiannouli, 2013)], *UAS-Ras85D^{wt}* from B.M. Mechler, Bam-GFP from Dennis McKearin, Rbp4-eGFP (Baker et al., 2015), α-Cat-YFP (CPTI-002510/DGRC115551) from the Kyoto Stock Center, *c587*-GAL4 (S. Hou, National Cancer Institute), *UAS-sktl-GFP* from Antoine Guichet (Gervais et al., 2008). Other fly stocks used in this study are described in FlyBase (www.flybase.org). All *UAS-gene^{RNAi}* stocks are referred to in the text as *gene^{RNAi}* for simplicity reasons. Knockdowns were performed using the *UAS-GAL4* system (Brand and Perrimon, 1993) by combining the *UAS-RNAi* fly lines with the cell-type specific *c587-GAL4* driver (Kai and Spradling, 2004) and *αtub-Gal80^{ts}* (Lee and Luo, 1999).

For the phenotypic analysis in adult *Drosophila* testes: *c587*-GAL4; *αtub-Gal80^{ts}; UAS-mCD8-GFP* or *c587*-GAL4*; αtub-Gal80^{ts}* flies were crossed to *UAS-gene^{RNAi}* flies. Crosses were raised at 18^{o}C until adult flies hatched. Then males with the correct genotype (along with few females) were shifted at 30^{o}C for 2-7 days depending on the experimental needs and the phenotypes were analyzed.

Immunofluorescence staining and microscopy

For whole mount testes immunostaining, testes were dissected in PBS, fixed for 20min in 8% formaldehyde and rinsed twice in 1% PBX (1% Triton-100x in PBS). Testes were permeabilized for 15 min in 1x PBS with 0.6% (vol/vol) Triton-100x and 0.6% (wt/vol) sodium deoxycholate at room temperature, washed twice with PBX and then blocked in 5% Bovine Serum Albumin in 1% PBX for 1h. Testes were incubated with primary antibodies over-night at 4^{o}C and the following day with the secondary antibodies for 2h at room temperature in the dark (Papagiannouli et al., 2014). For testes immunostaining in the presence of GFP, 1% PBT (1% Tween-20 in PBS) was used instead of 1% PBX in all steps. For the TUNEL assay, tissue was processed as described above except that after permeabilization, protocol from In Situ Cell Death Detection Kit (TMR Red, Sigma/Roche) was followed. For the dpERK staining testes were dissected in PBS including the phosphatase inhibitor cocktail 2 (1/100, Sigma P5726), were fixed in 4% formaldehyde including phosphatase inhibitor cocktail 2 (1/100) and all subsequent steps as described above. Testes were mounted in ProLong® Gold Antifade (Thermo Fischer Scientific).

The monoclonal antibodies used in this study: anti-Vasa (1/10; rat), anti-LamC-LC28.26 (1/10; mouse), anti-LamDm0-ADL101 (1/10; mouse), anti-Dlg (1/100, mouse) were obtained from the Developmental Studies Hybridoma Bank developed under the auspices of the NICHD and maintained by The University of Iowa, Department of Biological Sciences, Iowa City, IA 52242. Polyclonal anti-Vasa-dC13 (goat; 1/20) and mouse anti-pHistone H3 (C-2; 1/200) were from Santa Cruz Biotechnology, chicken anti-GFP (13970; 1/10,000) from Abcam and rabbit anti-Phospho-p44/42 MAPK (Erk1/2) (Thr202/Tyr204 #9101; 1/200) from Cell Signaling. Guinea-pig anti-TJ (1/5000) polyclonal antibody was a gift of Dorothea Godt, rabbit anti-Zfh1 (1/5000) was a gift of Ruth Lehmann. Filamentous (F-actin) was stained with Alexa Fluor phalloidin 546 or 647 (1/300, Thermo Fischer Scientific) and DNA with DAPI (Thermo Fischer Scientific). Following secondary antibodies were used: donkey anti-goat Alexa Fluor-488, donkey anti-mouse Alexa Fluor-546 and Alexa Fluor-647, donkey anti-guinea pig Alexa Fluor-546 and Alexa Fluor-647, donkey anti-rat Alexa Fluor-488, donkey anti-rabbit Alexa Fluor-488 and Alexa Fluor-546 from Thermo Fischer Scientific (1/500) and donkey anti-chicken Alexa Fluor-488 from Jackson ImmunoResearch (1/500).

Confocal images were obtained using a Leica SP8 system (1024x1024px, 184μm image frame) (CSIF Beckman Center, Stanford University School of Medicine; CECAD, University of Cologne). Pictures were finally processed with Adobe Photoshop 7.0. Quantifications were done using FiJi/ImageJ by measuring "Corrected Total Cell Fluorescence" (CTCF) [CTCF = Integrated Density - (Area of elected cell X Mean fluorescence of background readings)].

Dextran dye & permeability assays.
A dextran dye (3000MW) -biotin conjugated and fixable- was used to test the permeability of the testis barrier (Molecular Probes, D7135). Testes were dissected in Schneider 2 (S2) *Drosophila* medium with 8%FBS and then were incubated in dextran diluted in S2+8%PBS at a final concentration of 0.2µg/µl for 40min at 25oC. Testes were fixed in 8%FA for 20min and were subsequently stained with fluorescent streptavidin (Streptavidin, Alexa Fluor™ 546 conjugate; S11225; Thermo Scientific).

SUPPLEMENTAL REFERENCES
Baker, C.C., Gim, B.S., and Fuller, M.T. (2015). Cell type-specific translational repression of Cyclin B during meiosis in males. Development *142*, 3394-3402.
Brand, A.H., and Perrimon, N. (1993). Targeted gene expression as a means of altering cell fates and generating dominant phenotypes. Development *118*, 401-415.
Buszczak, M., Paterno, S., Lighthouse, D., Bachman, J., Planck, J., Owen, S., Skora, A.D., Nystul, T.G., Ohlstein, B., Allen, A.*, et al.* (2007). The carnegie protein trap library: a versatile tool for Drosophila developmental studies. Genetics *175*, 1505-1531.
Gervais, L., Claret, S., Januschke, J., Roth, S., and Guichet, A. (2008). PIP5K-dependent production of PIP2 sustains microtubule organization to establish polarized transport in the Drosophila oocyte. Development *135*, 3829-3838.
Kai, T., and Spradling, A. (2004). Differentiating germ cells can revert into functional stem cells in Drosophila melanogaster ovaries. Nature *428*, 564-569.
Lee, T., and Luo, L. (1999). Mosaic analysis with a repressible cell marker for studies of gene function in neuronal morphogenesis. Neuron *22*, 451-461.
Papagiannouli, F. (2013). The internal structure of embryonic gonads and testis development in Drosophila melanogaster requires scrib, lgl and dlg activity in the soma. Int J Dev Biol *57*, 25-34.
Papagiannouli, F., Schardt, L., Grajcarek, J., Ha, N., and Lohmann, I. (2014). The hox gene abd-B controls stem cell niche function in the Drosophila testis. Dev Cell *28*, 189-202.